International Journal of Thermophysics (2023) 44:180
https://doi.org/10.1007/s10765-023-03276-1

Highly Accurate Densities and Isobaric and Isochoric Heat Capacities of Compressed Liquid Water Derived from New Speed of Sound Measurements

Ahmed El Hawary[1] · **Karsten Meier**[1]

Received: 30 August 2023 / Accepted: 8 October 2023 / Published online: 20 November 2023

Abstract

Comprehensive and accurate measurements of the speed of sound in liquid water are reported. The measurements were carried out by a double-path-length pulse-echo technique and cover the temperature range from 273.65 K to 368.15 K with pressures up to 100 MPa. The relative expanded ($k = 2$) uncertainties are 2.1 mK in temperature, 45 parts-per-million (ppm) in pressure, and between 40 ppm and 70 ppm in speed of sound. Furthermore, values for the density and specific isobaric and isochoric heat capacities were derived from the speed of sound data in the measured temperature range up to 100 MPa by the method of thermodynamic integration. Very accurate values for the derived properties were obtained by using density data of Takenaka and Masui (Metrologia 27:165–171, 1990) and isobaric heat capacity data of Osborne et al. (J Res Natl Bur Stand 23:197, 1939) at ambient pressure as initial values in combination with an accurate correlation of our speed of sound. The relative expanded ($k = 2$) uncertainties of the derived properties are 2 ppm in density, 0.11% in isobaric heat capacity, and 0.12% in isochoric heat capacity. The experimental speeds of sound and derived properties are compared with experimental data of other authors from the literature, the IAPWS-95 (International Association of the Properties of Water and Steam) formulation for the thermodynamic properties of water, and a recent equation of state for supercooled water.

Keywords Liquid · Pulse-echo technique · Speed of sound · Thermodynamic integration · Water

Special Issue in Honor of Professor Roland Span's 60th Birthday.

✉ Karsten Meier
karsten.meier@hsu-hh.de

Ahmed El Hawary
a.elhawary@gmx.net

[1] Institut für Thermodynamik, Helmut-Schmidt-Universität/Universität der Bundeswehr Hamburg, Holstenhofweg 85, 22043 Hamburg, Germany

1 Introduction

In recent studies, we determined accurate values for the density and specific isobaric and isochoric heat capacities of *n*-butane, isobutane, and toluene by the method of thermodynamic integration from comprehensive speed of sound data sets [1, 2]. In these works, we showed that by a careful choice of values for the density and isobaric heat capacity on the initial isobar for the thermodynamic integration, values for the three properties with an uncertainty similar to that of the initial values can be derived. In this work, we report new speed of sound measurements in liquid water and apply the thermodynamic integration to this new data set to obtain values for the density and specific isobaric and isochoric heat capacities of water. In a similar work, Trusler and Lemmon [3] applied thermodynamic integration on a speed of sound data set for liquid water published by Lin and Trusler [4] to derive values for several thermodynamic properties of water. In that work, the initial values for the thermodynamic integration were calculated with the current reference equation of state (EOS) for water, the IAPWS-95 (International Association of the Properties of Water and Steam) formulation [5]. Since highly accurate experimental data for the density and isobaric heat capacity of water at ambient pressure are available, it is the aim of this work to show that values for the density and isobaric and isochoric heat capacities that are more accurate than the most accurate experimental data and values calculated with the IAPWS-95 formulation for these properties at high pressure can be derived by thermodynamic integration.

2 Experimental Procedure and Materials

For the measurements of the speed of sound, we used the speed of sound instrument developed by one of the authors [6]. Since it is described in detail in Refs. [6] and [7], only a brief description is given here. Our speed of sound sensor employs the double-path-length pulse-echo technique. The sound signals are generated by a piezoelectric quartz crystal, which operates at its resonance frequency of 8 MHz. The crystal is located with distances of about $L_1 = 20$ mm and $L_2 = 30$ mm between two stainless steel reflectors. It is excited by a sinusoidal burst signal and emits sound waves in both directions into the fluid. The signals are reflected at the reflectors and, because of the different distances, successively arrive at the crystal separated by a time difference Δt. The speed of sound c is determined as two times the difference of the distances divided by the measured time difference between the two received echoes by

$$c = \frac{2\Delta L}{\Delta t}, \tag{1}$$

where $\Delta L = L_2 - L_1$. Corrections to the time difference for diffraction effects were applied as described in Ref. [7]. The influence of thermal expansion on ΔL is taken into account by calibrating ΔL to highly accurate experimental data for the speed of

sound at ambient pressure at each measured isotherm as described below. The influence of the compression of the sensor under pressure on ΔL is accounted for by

$$\Delta L(T,p) = \Delta L(T,p_0) - \frac{1}{E(T)}(1-2\nu)(p-p_0), \tag{2}$$

in which T is temperature, p is pressure, p_0 is the ambient pressure, and E and ν denote the elastic modulus and the Poisson number of the sensor material, respectively. The speed of sound sensor is housed in a pressure vessel capable of pressures up to 100 MPa. The pressure vessel is thermostatted in a circulating liquid-bath thermostat with silicone oil with a temperature stability better than 0.5 mK. The temperature is measured in the wall of the pressure vessel with a long-stem 25.5 Ω standard platinum resistance thermometer calibrated on the ITS-90 at the Physikalisch-Technische Bundesanstalt in Berlin. The pressure is measured with a pressure balance operated with nitrogen, which is coupled to the water by a differential pressure null indicator. Measurements at ambient pressure are performed with the nitrogen side of the differential pressure indicator open to the environment. For each measured state, a detailed uncertainty analysis was carried out as described in Ref. [1]. In this work, uncertainties are reported as expanded uncertainties with a coverage factor $k = 2$, which corresponds to the 0.95 confidence level. The expanded ($k = 2$) uncertainty in the temperature measurement is 2.1 mK, while the relative expanded ($k = 2$) uncertainty in the pressure measurement amounts to 45 parts per million (ppm) of the measured value. The contributions to the uncertainty in the speed of sound due to the uncertainty in the pressure and temperature measurements were estimated by the IAPWS-95 formulation [5]. The combined relative expanded ($k = 2$) uncertainty in the speed of sound increases from 40 ppm at ambient pressure to 70 ppm at 100 MPa. These estimates include the uncertainty in the calibration of the path length, in the time measurement, in the diffraction correction, in the compression of the speed of sound sensor under pressure, and contributions due to the uncertainty in the temperature and pressure measurements.

The water samples were obtained from tap water, which was deionized by a water purifier (arium comfort, Sartorius Lab Instruments) and subsequently degassed under vacuum. The purifier delivers a water quality of ASTM type 1 [8]. The isotopic composition of the purified water was determined at the company Beta Analytic in Miami, FL, U.S.A, on the Vienna Standard Mean Ocean Water–Standard Light Antarctic Precipitation (VSMOW-SLAP) scale [9] using cavity ring-down spectroscopy in terms of δ^{17}O, δ^{18}O, and δ^{2}H ratios to be $\delta^{17}\mathrm{O} = -4.03$ parts per thousand (ppt), $\delta^{18}\mathrm{O} = -7.86$ ppt, and $\delta^{2}\mathrm{H} = -52.64$ ppt with expanded ($k = 2$) uncertainties 0.06 ppt, 0.02 ppt, and 0.12 ppt, respectively. The measurements were carried out along isotherms. For each measured isotherm a new water sample was prepared to keep changes of the water purity due to corrosion of the parts of the apparatus in contact with the water to a minimum. After the measurements at an isotherm were completed, the path length in our sensor at the temperature of the isotherm was calibrated using the measurement at ambient pressure. With the data of Del Grosso and Mader [10], Fujii and Masui [11], and Kroebel and Mahrt [12] three very accurate data sets for the speed of sound

in water at ambient pressure are available, which can be used as references for the calibration. The data of Kroebel and Mahrt cover the temperature range from 276.49 K to 306.95 K, the data of Fujii and Masui the range from 292.99 K to 347.83 K, and the data of Del Grosso and Mader the range between 273.15 K and 368.28 K. The uncertainty of the data were estimated by Kroebel and Mahrt to be 28 ppm, by Fujii and Masui to be 9 ppm, and by Del Grosso and Mader to be 11 ppm. Despite the rather low uncertainty reported by Del Grosso and Mader as well as Fujii and Masui, the data near 293 K differ by about up to 30 ppm. Marczak [13] discussed this difference and suggested that they are due to different purities of the water samples. Another reason for the difference could be a different isotopic composition of the water samples. Since at the time the three works were published the concept of standard and expanded ($k = 2$) uncertainties was not generally used, it is not clear which value of k should be assigned to each data set. We used the data of Del Grosso and Mader as reference because they cover the largest temperature range of the three data sets, and we estimate the expanded ($k = 2$) uncertainty of these data to be 30 ppm, which corresponds to the largest difference between the data of Del Grosso and Mader and Fujii and Masui. Figure 1 depicts relative deviations of our measurements at ambient pressure after the calibration and deviations of the three data sets from the literature from the IAPWS-95 formulation as a function of temperature. Figure 1 shows that our measurements agree with the data of Del Grosso and Mader mostly within the scatter of the data.

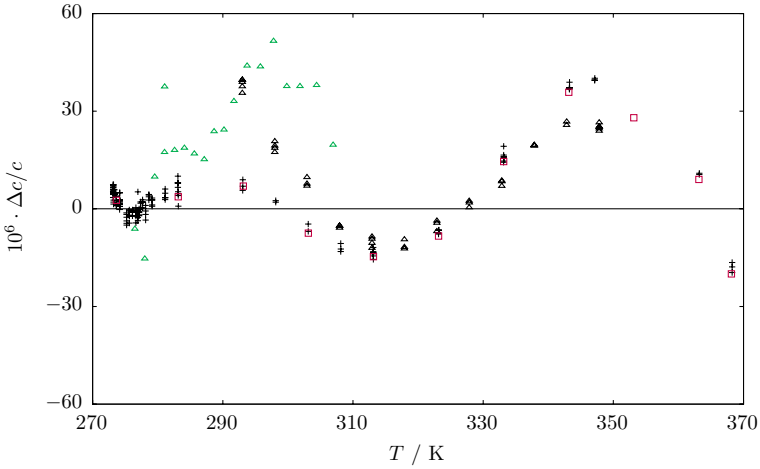

Fig. 1 Relative deviations of our experimental speeds of sound in water at ambient pressure after the calibration and of data from the literature from values calculated with the IAPWS-95 formulation as a function of temperature. Experimental data: □, this work; +, Del Grosso and Mader [10]; △, Kroebel and Mahrt [12]; and △, Fujii and Masui [14]

3 Experimental Results

In this work, 151 speed of sound measurements were carried out in water, including eight measurements on two isotherms to check the reproducibility. The distribution of our measurements and the most accurate data of other authors from the literature for the speed of sound in water in the pressure-temperature diagram is shown in Fig. 2. Our measurements were carried out along the isotherm 273.65 K, between 283.15 K and 363.15 K along isotherms in steps of 10 K, and along the isotherm 368.15 K from ambient pressure up to 100 MPa. The experimental results including the combined expanded ($k = 2$) uncertainty in speed of sound are reported in Tables 1 and 2. All check measurements agree within 4 ppm with the values of the main measurement campaign with the exception of one measurement at 313.15 K and ambient pressure, where the difference is 17 ppm. Thus, the reproducibility is well within the estimated uncertainty.

For the application of thermodynamic integration in Sect. 4, a correlation of the data is required, which describes the square of the speed of sound in the region of the measurements as a function of temperature and pressure. The functional form of the correlation was established with the linear structural optimization technique devised by Wagner [28]. The optimized correlation for the speed of sound squared

$$\left[c(p,T)\right]^2 = \sum_{i=1}^{12} a_i \left(\frac{p}{p_\mathrm{c}}\right)^{m_i} \left(\frac{T}{T_\mathrm{c}}\right)^{n_i} \tag{3}$$

consists of 12 double polynomial terms in temperature and pressure, where the values of the coefficients a_i and exponents m_i and n_i were obtained by the structural optimization procedure. $T_\mathrm{c} = 647.096\,\mathrm{K}$ and $p_\mathrm{c} = 22.064\,\mathrm{MPa}$ denote the critical temperature and critical pressure of water, respectively [5]. The values of the coefficients a_i and exponents m_i and n_i of the terms are listed in Table 3. Figure 3 depicts relative deviations of our data from the correlation at isobars and isotherms. It is evident that the correlation represents our data within 25 ppm with only few exceptions in the whole range of our measurements. The expanded ($k = 2$) uncertainty in the correlation is conservatively estimated to be 90 ppm.

The measured speed of sound isotherms are plotted in Fig. 4 as a function of pressure. In the range of our measurements, the speed of sound takes values from about $1400\,\mathrm{m \cdot s^{-1}}$ to $1750\,\mathrm{m \cdot s^{-1}}$. At all measured isotherms, the speed of sound increases nearly linearly with pressure. At ambient pressure, the speed of sound exhibits a maximum near 347 K. With increasing pressure, the maximum is shifted to higher temperatures and is reached at about 361 K at 100 MPa.

In the following, our experimental speed of sound isotherms are compared with the data sets from the literature shown in Fig. 2 at temperatures near those of our measured isotherms, the IAPWS-95 formulation [5], and the EOS of Holten et al. [29]. Details of the data sets from the literature are summarized in Table 4. The literature search was carried out with the help of the NIST ThermoDataEngine database [30]. The IAPWS-95 formulation is the current reference EOS for water [31]. The relative expanded ($k = 2$) uncertainty in speeds of sound calculated with the formulation was originally estimated by Wagner and Pruß to be 0.005% at ambient

Table 1 Experimental values for the speed of sound c in liquid water and combined expanded ($k = 2$) uncertainty in the speed of sound U_c as a function of temperature T and pressure p

T / K	p / MPa	c / m · s^{-1}	$U_c(c)$ / m · s^{-1}	T / K	p / MPa	c / m · s^{-1}	$U_c(c)$ / m · s^{-1}
$T = 273.65$ K							
273.6459	0.102385	1404.87	0.06	273.6460	50.1358	1487.90	0.08
273.6459	5.10244	1412.49	0.06	273.6461	60.1425	1505.84	0.09
273.6461	10.1090	1420.28	0.06	273.6459	70.1493	1523.98	0.09
273.6459	15.1123	1428.25	0.06	273.6460	80.1558	1542.32	0.10
273.6461	20.1157	1436.39	0.07	273.6459	90.1624	1560.75	0.10
273.6460	30.1223	1453.08	0.07	273.6460	100.169	1579.22	0.11
273.6461	40.1291	1470.29	0.08				
$T = 283.15$ K							
283.1497	0.102814	1447.28	0.06	283.1495	50.1355	1530.31	0.08
283.1499	5.10202	1455.21	0.06	283.1497	60.1421	1547.60	0.09
283.1499	10.1093	1463.26	0.06	283.1500	70.1487	1565.00	0.09
283.1496	15.1126	1471.37	0.07	283.1495	80.1558	1582.47	0.10
283.1495	20.1156	1479.59	0.07	283.1496	90.1625	1599.96	0.10
283.1493	30.1222	1496.25	0.07	283.1496	100.169	1617.46	0.11
283.1493	40.1289	1513.16	0.08				
$T = 293.15$ K							
293.1521	0.100549	1482.36	0.06	293.1528	50.1344	1565.70	0.09
293.1521	5.10542	1490.58	0.06	293.1523	60.1411	1582.60	0.09
293.1525	10.1072	1498.79	0.07	293.1522	70.1479	1599.48	0.10
293.1530	15.1106	1507.04	0.07	293.1520	80.1546	1616.43	0.10
293.1527	20.1139	1515.34	0.07	293.1517	90.1613	1633.31	0.11
293.1527	30.1205	1532.05	0.08	293.1516	100.168	1650.19	0.11
293.1522	40.1272	1548.82	0.08				
$T = 303.15$ K							
303.1469	0.103248	1509.14	0.06	303.1461	50.1385	1593.19	0.09
303.1469	5.10666	1517.55	0.06	303.1461	60.1454	1609.94	0.09
303.1468	10.1100	1525.97	0.07	303.1460	70.1523	1626.63	0.10
303.1469	15.1134	1534.38	0.07	303.1463	80.1590	1643.24	0.10
303.1467	20.1168	1542.79	0.07	303.1463	90.1659	1659.80	0.11
303.1456	30.1244	1559.61	0.08	303.1464	100.173	1676.26	0.11
303.1460	40.1315	1576.42	0.08				
$T = 313.15$ K							
313.1469	0.103525	1528.88	0.06	313.1471	50.1384	1614.20	0.09
313.1469	5.10359	1537.52	0.07	313.1471	60.1453	1630.96	0.09
313.1471	10.1104	1546.16	0.07	313.1472	70.1522	1647.58	0.10
313.1473	15.1138	1554.75	0.07	313.1476	80.1590	1664.10	0.11
313.1475	20.1173	1563.32	0.07	313.1475	90.1658	1680.47	0.11
313.1474	30.1242	1580.39	0.08	313.1478	100.173	1696.77	0.12
313.1469	40.1315	1597.34	0.08				

Table 1 (continued)

T / K	p / MPa	c / m · s^{-1}	$U_c(c)$ / m · s^{-1}	T / K	p / MPa	c / m · s^{-1}	$U_c(c)$ / m · s^{-1}
$T = 323.15$ K							
323.1474	0.10201	1542.56	0.06	323.1466	50.1369	1629.53	0.09
323.1470	5.10217	1551.45	0.07	323.1456	60.1443	1646.41	0.10
323.1468	10.1090	1560.32	0.07	323.1461	70.1512	1663.10	0.10
323.1471	15.1125	1569.12	0.07	323.1456	80.1580	1679.66	0.11
323.1469	20.1160	1577.90	0.07	323.1459	90.1648	1696.02	0.11
323.1468	30.1230	1595.29	0.08	323.1459	100.172	1712.26	0.12
323.1470	40.1300	1612.50	0.08				
$T = 333.15$ K							
333.1506	0.103332	1551.00	0.06	333.1504	50.1373	1640.12	0.09
333.1505	5.10336	1560.21	0.07	333.1499	60.1441	1657.20	0.10
333.1504	10.1102	1569.36	0.07	333.1499	70.1509	1674.10	0.10
333.1506	15.1136	1578.43	0.07	333.1501	80.1577	1690.77	0.11
333.1503	20.1170	1587.42	0.07	333.1502	90.1646	1707.26	0.11
333.1504	30.1239	1605.24	0.08	333.1502	100.171	1723.55	0.12
333.1501	40.1309	1622.80	0.09				
$T = 343.15$ K							
343.1499	0.103922	1554.81	0.06	343.1492	50.1384	1646.41	0.09
343.1503	5.10397	1564.35	0.07	343.1492	60.1452	1663.83	0.10
343.1499	10.1109	1573.81	0.07	343.1490	70.1520	1680.98	0.10
343.1494	15.1143	1583.18	0.07	343.1492	80.1588	1697.87	0.11
343.1492	20.1178	1592.45	0.07	343.1489	90.1655	1714.54	0.11
343.1493	30.1247	1610.75	0.08	343.1488	100.172	1730.98	0.12
343.1492	40.1316	1628.73	0.09				
$T = 353.15$ K							
353.1448	0.104249	1554.48	0.06	353.1536	50.1386	1648.92	0.09
353.1535	5.10421	1564.39	0.07	353.1538	60.1456	1666.72	0.10
353.1536	10.1109	1574.19	0.07	353.1537	70.1526	1684.21	0.10
353.1538	15.1143	1583.87	0.07	353.1536	80.1596	1701.40	0.11
353.1537	20.1178	1593.46	0.07	353.1534	90.1666	1718.33	0.11
353.1535	30.1247	1612.31	0.08	353.1532	100.174	1735.00	0.12
353.1538	40.1317	1630.78	0.09				
$T = 363.15$ K							
363.1451	0.103474	1550.47	0.06	363.1472	50.1369	1648.09	0.09
363.1451	5.10694	1560.78	0.07	363.1475	60.1415	1666.34	0.10
363.1452	10.1108	1570.97	0.07	363.1477	70.1479	1684.24	0.10
363.1455	15.1143	1581.02	0.07	363.1479	80.1542	1701.81	0.11
363.1460	20.1177	1590.94	0.07	363.1478	90.1603	1719.07	0.11
363.1456	30.1244	1610.43	0.08	363.1475	100.167	1736.03	0.12
363.1465	40.1306	1629.47	0.09				
$T = 368.15$ K							
368.1452	0.100724	1547.17	0.06	368.1448	50.1345	1646.52	0.09

Table 1 (continued)

T / K	p / MPa	c / m · s^{-1}	$U_c(c)$ / m · s^{-1}	T / K	p / MPa	c / m · s^{-1}	$U_c(c)$ / m · s^{-1}
368.1454	5.09986	1557.69	0.07	368.1448	60.1412	1665.04	0.10
368.1449	10.1075	1568.09	0.07	368.1446	70.1480	1683.17	0.10
368.1449	15.1109	1578.33	0.07	368.1448	80.1549	1700.93	0.11
368.1447	20.1143	1588.43	0.07	368.1448	90.1617	1718.39	0.11
368.1450	30.1210	1608.26	0.08	368.1446	100.169	1735.52	0.12
368.1448	40.1277	1627.62	0.09				

Expanded ($k = 2$) uncertainties: $U(T) = 2.1$ mK and $U(p) = 45 \times 10^{-6} p$

Table 2 Experimental values for the speed of sound c in liquid water of the check measurements and combined expanded ($k = 2$) uncertainty in the speed of sound U_c as a function of temperature T and pressure p

T / K	p / MPa	c / m · s^{-1}	$U_c(c)$ / m · s^{-1}	T / K	p / MPa	c / m · s^{-1}	$U_c(c)$ / m · s^{-1}
$T = 313.15$ K							
313.1489	0.103016	1528.86	0.06	313.1467	30.1245	1580.40	0.08
313.1488	10.1097	1546.16	0.07	313.1489	50.1368	1614.20	0.09
313.1487	30.1232	1580.40	0.08				
$T = 323.15$ K							
323.1477	0.103011	1542.56	0.06	323.1480	50.1366	1629.53	0.09
323.1476	10.1097	1560.32	0.07				

Expanded ($k = 2$) uncertainties: $U(T) = 2.1$ mK and $U(p) = 45 \times 10^{-6} p$

pressure, 0.03% from 303.15 K to 323.15 K up to 100 MPa, and 0.1% at lower and higher temperatures up to 100 MPa in the temperature range of our measurements [5]. The EOS of Holten et al. [29] was mainly developed to represent the properties of supercooled water and is recommended by IAPWS as reference EOS for supercooled water [32]. It is valid from the homogeneous ice nucleation temperature up to 300 K with pressures up to 400 MPa. The expanded ($k = 2$) uncertainties in the speed of sound in the liquid phase at temperatures above the triple point temperature are 0.002% at ambient pressure, 0.02% up to 60 MPa, and 0.05% at higher pressures.

This comparison includes only data sets that overlap with the region of our measurements, but does not consider data sets at higher temperatures [33–37], higher pressures [38–42], or in saturated liquid water [43]. Also not included is the work of Litovitz and Carnevale [44] since they published only four data points at 303.15 K, whose uncertainty is much higher than that of the data sets listed in Table 4. Belogolskii et al. [45] performed measurements in the temperature range between 273.15 K and 323.15 K up to 60 MPa, but they did not publish the original experimental data but values calculated with a correlation fitted to the data. Moreover, the data of Vance and Brown [46] were superseded regarding accuracy by the data of Bollengier et al. [20] from the same group, and the data of Gedanitz et al. [47] are of similar accuracy as the data of Meier and Kabelac [7] and Fujii [11], but cover

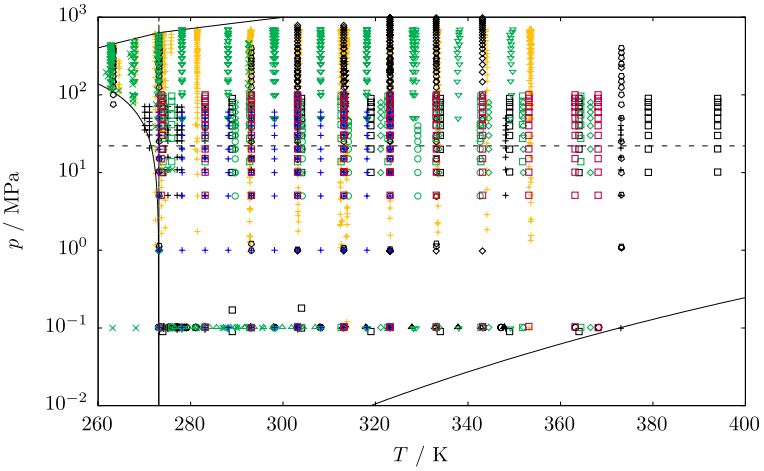

Fig. 2 Distribution of our measurements and experimental data for the speed of sound of other authors in liquid water from the literature in a pressure–temperature diagram. The critical point is at (647.10 K, 22.064 MPa), and the triple point is at (273.16 K, 0.612 kPa) [5]. Experimental data: □, this work; ×, Aleksandrov and Kochetov [15]; +, Aleksandrov and Larkin [16]; ▽, Baltasar et al. [17]; ◇, Barlow and Yazgan [18]; □, Benedetto at al. [19]; +, Bollengier et al. [20]; ○, Del Grosso and Mader [10]; +, Fehres [21]; ▽, Fujii [11]; △, Fujii and Masui [14]; ◇, Holton et al. [22]; △, Kroebel and Mahrt [12]; ⬡, Lago [23]; ⬡, Lin and Trusler [4]; ○, Meier and Kabelac [6]; ×, Petitet et al. [24]; □, Wilson [25]; ○, Ye et al. [26]; - - - -, triple point temperature and critical pressure calculated with the IAPWS-95 formulation; and ——, vapor and melting pressure curves calculated with the IAPWS-95 formulation and the reference equation for the melting pressure of Wagner et al. [27], respectively

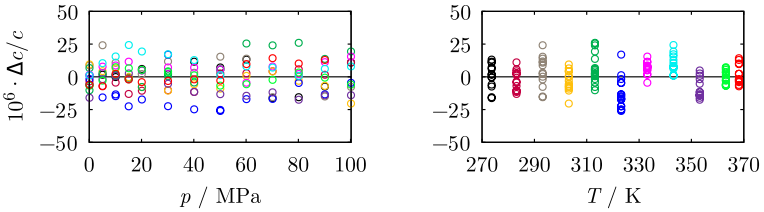

Fig. 3 Relative deviations of our experimental speeds of sound in water from values calculated with the speed of sound correlation (Eq. 3) as a function of pressure (left) and temperature (right). Experimental data: ○, 273.65 K; ○, 283.15 K; ○, 293.15 K; ○, 303.15 K; ○, 313.15 K; ○, 323.15 K; ○, 333.15 K; ○, 343.15 K; ○, 353.15 K; ○, 363.15 K; and ○, 368.15 K

only pressures up to 30 MPa. Among the numerous works in the literature, in which the speed of sound in water was measured at ambient pressure, only the works of Del Grosso and Mader [10], Kroebel and Mahrt [12], and Fujii and Masui [14] are included in Table 4 because they provided the most accurate data.

Figure 5 shows relative deviations of our measurements, our speed of sound correlation (Eq. 3), the EOS of Holten et al. [29] and selected data of other authors from the literature [4, 7, 10–12, 14–26] from the IAPWS-95 formulation as a function of pressure along isotherms. Our data are very consistent, agree with the IAPWS-95

Table 3 Values of the coefficients a_i and exponents m_i and n_i in the speed of sound correlation (Eq. 3)

i	a_i	m_i	n_i
1	$7.423615233 \times 10^{4}$	0	− 5.0
2	$-1.571527759 \times 10^{5}$	0	− 4.5
3	$2.742740269 \times 10^{6}$	0	− 0.5
4	$-3.599403339 \times 10^{6}$	0	3.5
5	$-6.379367333 \times 10^{-4}$	1	− 19.0
6	$2.357819770 \times 10^{5}$	1	1.0
7	$5.469994955 \times 10^{5}$	1	7.0
8	$2.225433179 \times 10^{-1}$	2	− 12.0
9	$-2.304269454 \times 10^{5}$	2	8.0
10	$3.932184362 \times 10^{-7}$	3	− 26.0
11	$-2.621801558 \times 10^{-6}$	3	− 24.0
12	$2.991452743 \times 10^{5}$	3	14.0

formulation within its uncertainty on all isotherms, and show the same pressure dependence as the data of Fujii [11], Meier and Kabelac [7], and Fehres [21], with which they agree best. The largest deviations from the IAPWS-95 formulation are observed at low temperature and high pressure. Between 273.65 K and 303.15 K, the deviation pattern is similar. The deviations are negative at low pressure, decrease with pressure to a minimum at about 25 MPa, become positive between 30 MPa and 60 MPa, and reach their largest values at 100 MPa. The deviations at 100 MPa are +0.084% at 273.65 K, +0.090% at 283.15 K, +0.058% at 293.15 K, and +0.022% at 303.15 K. Between 313.15 K and 333.15 K, our data agree with the IAPWS-95 formulation within 0.014%. The largest deviations are observed between 30 MPa and 60 MPa. At 343.15 K, the agreement with the IAPWS-95 formulation is within 40 ppm in the whole pressure range of our measurements. At 353.15 K, 363.15 K and 368.15 K, the deviations increase again with pressure and reach the largest values at 100 MPa, where they amount to between +0.013% and +0.028%.

Our data agree with the data of Meier and Kabelac, which were measured with the same apparatus as the present measurements in 2005, within 45 ppm. This agreement is within the uncertainties of both data sets. Speeds of sound calculated with the Holten et al. EOS generally agree with our data within 0.01%. At 273.65 K, the deviations of our data from the Holten et al. EOS remain within 30 ppm up to 50 MPa and reach +0.012% at 100 MPa. At 283.15 K and 293.15 K, the agreement is within 65 ppm. At 303.15 K, which is slightly above the range of validity of the Holten et al. EOS, the deviations increase up to +100 ppm above 20 MPa. Our data agree with those of Fehres [21] mostly within their very low relative expanded ($k = 2$) uncertainty of 30 ppm except for the data at 283.15 K, where the deviations increase up to 42 ppm. These data also agree well with the Holten et al. EOS. The good agreement between our data, the Fehres data, and the Holten et al. EOS confirms the high accuracy of our measurements.

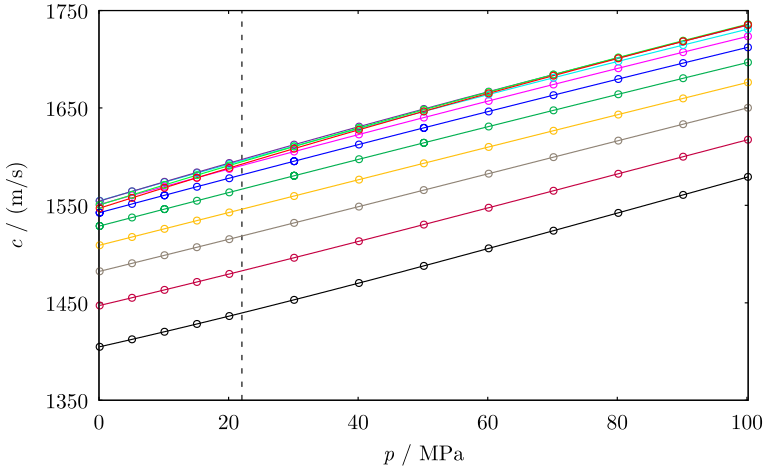

Fig. 4 Experimental speeds of sound in water as a function of pressure. Lines represent speeds of sound calculated with the speed of sound correlation (Eq. 3). Experimental data: ○, 273.65 K; ○, 283.15 K; ○, 293.15 K; ○, 303.15 K; ○, 313.15 K; ○, 323.15 K; ○, 333.15 K; ○, 343.15 K; ○, 353.15 K; ○, 363.15 K; and ○, 368.15 K

Table 4 Details of experimental data sets of other authors for the speed of sound in liquid water from the literature. In all works, the pulse-echo method was applied

Author	Year	f / MHz	Data	T /K	p / MPa	$U_r(c)$ / %
Lago [23]	2023		4	273	1–100	0.02
Fehres [21]	2021	2.5	110	273–323	0.1–60	0.003−0.008
Bollengier [20]	2019	3–7	901	253–353	0.1–700	0.02−0.034
Lin [4]	2012	5	213	253–473	1.0–401	0.03−0.04
Baltasar [17]	2011	2	447	253–348	0.1–705	0.22−0.32
Meier [7]	2006	8	33	303–323	0.1−100.2	0.003−0.0055
Benedetto [19]	2005	5	90	274–394	0.09−90.1	0.11
Fujii [11]	1994	17.2	47	303–323	0.1−199.9	0.01
Fujii [14]	1993	16.5	41	293–348	0.1	0.001
Ye [26]	1990	5	45	290–343	5.0−47.2	0.06
Petitet [24]	1983	5	105	253–296	0.1−461.6	0.05
Aleksandrov [15]	1979	2.5 / 5.6	60	266–423	6.0−99.1	0.05
Aleksandrov [16]	1976	3	195	270–647	0.09−70.65	0.05
Kroebel [12]	1976	4	20	276–307	0.1	0.003
Del Grosso [10]	1972	5	148	273–368	0.1	0.001
Holton [22]	1968	15	34	273–343	0.98−982.5	0.2
Barlow [18]	1967	10	72	290–367	0.1–80	0.04
Wilson [25]	1959	5	88	274–364	0.1−96.5	0.05

Fig. 5 Relative deviations of our experimental speeds of sound, our speed of sound correlation (Eq. 3), ▶ the equation of state of Holten et al. [29], and selected experimental data of other authors from the literature from values calculated with the IAPWS-95 formulation as a function of pressure. Experimental data: □, this work; ×, Aleksandrov and Kochetov [15]; +, Aleksandrov and Larkin [16]; ▽, Baltasar et al. [17]; ◇, Barlow and Yazgan [18]; □, Benedetto at al. [19]; +, Bollengier et al. [20]; ○, Del Grosso and Mader [10]; +, Fehres [21]; ▽, Fujii [11]; △, Fujii and Masui [14]; ◇, Holton et al. [22]; △, Kroebel and Mahrt [12]; ⬡, Lago [23]; ⬡, Lin and Trusler [4]; ○, Meier and Kabelac [6]; ×, Petitet et al. [24]; □, Wilson [25]; and ○, Ye et al. [26]. Correlations: ——, speed of sound correlation (Eq. 3) and - - - -, EOS of Holten et al. [29]. The relative ($k = 2$) uncertainty in our data increases from 40 ppm at ambient pressure to 70 ppm at 100 MPa. The relative ($k = 2$) uncertainty in the IAPWS-95 formulation is 0.03% between 303.15 K and 323.15 K and 0.1% at higher temperatures in the region of our measurements

The data of Lin and Trusler [4] also exhibit a similar dependence on pressure as ours. The agreement is mostly within 35 ppm at the isotherm 293.15 K, where Lin and Trusler calibrated their sensor at 1 MPa with a speed of sound value calculated with the IAPWS-95 formulation. The path length in their sensor at other temperatures was calculated by using values for the material properties of the sensor parts from the literature. On some isotherms, their data are systematically lower than ours by between up to 0.015% at 303.15 K and 333.15 K and 0.03% at 273.65 K and 313.15 K, while at 323.15 K and 368.15 K they are up to 0.02% higher than our data. The data of Benedetto et al. [19] show a similar dependence on pressure as our data and the data of Fehres, Fujii, and Meier and Kabelac, but are systematically lower than our data by up to 0.03% between 273.65 K and 353.15 K and systematically higher than ours at 363.15 K and 368.15 K by 0.015% and 0.005%, respectively. The reason for the systematic differences is probably that they measured the path length in their sensor at ambient temperature and pressure with a coordinate measuring machine and, thus, performed absolute measurements. The expansion of their sensor with temperature and compression under pressure was calculated by using values for the thermal expansion coefficient and compressibility of the sensor material from the literature. This procedure was probably less accurate than a calibration using the highly accurate data at ambient pressure as reference. The data of Bollengier et al. [20] are also very accurate, but scatter somewhat more than the Lin and Trusler data and the Benedetto et al. data. They agree with our data within 0.03%. The data of Aleksandrov and Larkin [16] agree with our data within 0.05% at 273.65 K and within 0.02% at higher temperatures. They also exhibit a similar pressure dependence as our data on all isotherms except at 353.15 K, where the deviations from our data increase with pressure. The four data points of Lago et al. [23] at 273.64 K are also very accurate and agree with our data within 0.015%.

All other data sets listed in Table 4 show larger deviations from our data. The data of Wilson [25] are systematically higher than our data by between 0.02% and 0.1%. The data of Aleksandrov and Kochetov [15] show some scatter and deviate from our data by up to 0.1%. The data of Ye et al. [26] scatter more than our data and agree with them within 0.06%. From the data set of Petitet et al. [24], only a few data points lie in the region of our measurements. They scatter more than the

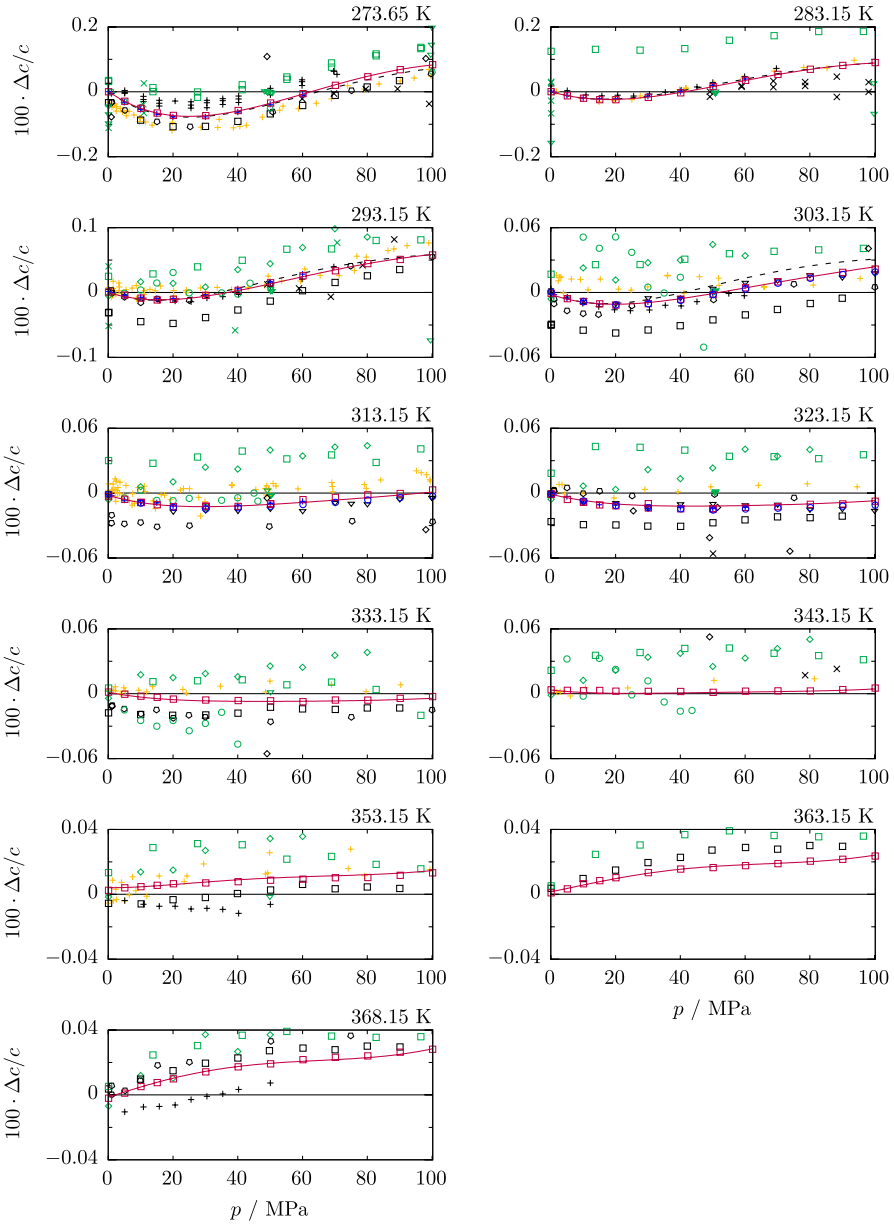

data of the other authors, but agree with ours within 0.1%. The data of Barlow and Yazgan [22] agree better with the data of Wilson than with ours, but scatter more than Wilson's data. The data of Holten et al. [22] and Baltasar et al. [17] show larger deviations from our data than the data of the other authors and lie mostly outside the scale of the plots.

4 Derived Properties

The method of thermodynamic integration was applied on our speed of sound data to derive highly accurate values for the density ρ and isobaric and isochoric heat capacities, c_p and c_v, of water. When the speed of sound in a fluid is known in a certain region of temperature and pressure, the thermodynamic relations

$$\left(\frac{\partial \rho}{\partial p}\right)_T = \frac{1}{c^2} + \frac{T}{\rho^2 c_p} \cdot \left(\frac{\partial \rho}{\partial T}\right)_p^2 \tag{4}$$

$$\left(\frac{\partial c_p}{\partial p}\right)_T = -\frac{T}{\rho^3}\left[2\left(\frac{\partial \rho}{\partial T}\right)_p^2 - \rho\left(\frac{\partial^2 \rho}{\partial T^2}\right)_p\right] \tag{5}$$

can be interpreted as partial differential equations for the unknown functions $\rho(T,p)$ and $c_p(T,p)$ [48]. When supplemented with initial values for the density and isobaric heat capacity at an isobar, a well-posed initial value problem is formulated that can be solved by numerical integration of Eqs. 4 and 5.

In previous works, we applied this method to determine values for the density and specific heat capacities of liquid isobutane [1] and toluene and *n*-butane [2] from accurate speed of sound measurements. In both works, the initial values for the density and isobaric heat capacity were derived from very accurate density data by the method described by El Hawary and Meier [1]. Since for water very accurate experimental data for the density and isobaric heat capacity at ambient pressure are available, these data can directly be used as initial values. Here, the density data of Takenaka and Masui [49] and isobaric heat capacity data of Osborne et al. [50] at ambient pressure are used as initial values because they are very accurate and cover a large part of the temperature range of our speed of sound measurements. Thus, the isobar 101.325 kPa was chosen as initial isobar for the thermodynamic integration.

Takenaka and Masui [49] measured the thermal expansion of water in the temperature range between 273.15 K and 358.15 K by a dilatometric technique and developed a correlation for the ratio of the density and the maximum density at 101.325 kPa. The uncertainty of the correlation was estimated to be 1 ppm. The measurements of Takenaka and Masui were carried out using purified tap water with natural isotopic composition, whose density is 1.6 ppm lower than the density of Vienna Standard Mean Ocean Water given by the Bureau International des Poids et Mesures (BIPM). The maximum density of the purified tap water samples was 999.9734 $\mathrm{kg \cdot m^{-3}}$, while the value for VSMOW given by the BIPM is 999.975 $\mathrm{kg \cdot m^{-3}}$ [51]. Masui et al. [52] later determined the value 999.9756 $\mathrm{kg \cdot m^{-3}}$ for the maximum density of VSMOW with an expanded ($k = 2$) uncertainty of 0.0016 $\mathrm{kg \cdot m^{-3}}$. Since this value agrees with the value for VSMOW given by the BIPM within its uncertainty, we calculated the initial densities for the thermodynamic integration between 273.65 K and 358.15 K with the correlation of Takenaka and Masui, Eq. 4 in Ref. [49],

$$\frac{\rho(\vartheta)}{999.975\ \mathrm{kg\cdot m^{-3}}} = 1 - \frac{(\vartheta - 3.98152)^2(\vartheta + 396.18534)(\vartheta + 32.28853)}{609628.6(\vartheta + 83.12333)(\vartheta + 30.24455)}, \quad (6)$$

in which ϑ denotes the Celsius temperature, using the value for the maximum density of VSMOW given by the BIPM. The same procedure was applied by Wagner and Pruß to determine values for the density of water at ambient pressure for the development of the IAPWS-95 formulation. At 363.15 K and 368.15 K, densities were calculated with the IAPWS-95 formulation and increased by 1 ppm so that their deviations from the IAPWS-95 formulation closely follow the trend of the deviations of the correlation of Takenaka and Masui.

The data of Osborne et al. [50] for the isobaric heat capacity were measured by an adiabatic calorimeter in the temperature range between 273.15 K and 373.15 K at 101.325 kPa in small temperature steps of 1 K. Thus, initial values for the isobaric heat capacity were interpolated by polynomial fits to the data reported in Table 6 of Ref. [50].

Relative deviations of the selected initial values and data of other authors for the density and isobaric heat capacity from the literature from the IAPWS-95 formulation are shown in Fig. 6. Beside deviations of the experimental data of Takenaka and Masui [49] and Masui et al. [52], also deviations of data published by Wolf et al. [53], Patterson and Morris [55], and Tanaka et al. [54] are shown in Fig. 6. The data of Tanaka et al. are recommended values for the density of water at 101.325 kPa between 273.15 K and 313.15 K obtained from the analysis of several experimental data sets. These data have a relative expanded ($k = 2$) uncertainty of 0.9 ppm and are currently considered to be the most accurate data for the density of water at 101.325 kPa. All data sets show the same temperature dependence at low temperatures between 273 K and 290 K. The deviations exhibit a maximum at about 283 K. The data of Masui et al. are 0.6 ppm higher than our initial values and the data of Tanaka et al. and Takenaka and Masui, while the data of Patterson and Morris lie about 1 ppm below our initial values and the data of Takenaka and Masui and Masui et al. At about 300 K, the deviations of all data except those of Tanaka et al. exhibit a shallow minimum. At higher temperatures, the deviations of the data of Takenaka and Masui and Masui et al. increase, but remain below 1.3 ppm and 2 ppm, respectively. From this comparison, we estimate the relative expanded ($k = 2$) uncertainty in initial values to be 2 ppm.

The deviations of the data of Osborne et al. for the isobaric heat capacity, and hence of our initial values, from the IAPWS-95 formulation do not exceed 0.08% and show a minimum at 283 K, where the deviations of the density data and speed of sound data in Fig. 1 exhibit a maximum. These observations indicate that there is an interdependence between the deviations of the speed of sound, density, and isobaric heat capacity data, which is probably caused by a small systematic error in the IAPWS-95 formulation. The data of Angell et al. [67], Anouti et al. [64], García-Miaja et al. [65], Gómez-Álvarez et al. [57], Shokouhi et al. [58], and Shokouhi et al. [59] tend to scatter, but agree with the data of Osborne et al. within 0.05% except for the data of Anouti et al. above 350 K and one value of García-Miaja et al. at 288 K. The data of He et al. [56], Wasiak et al. [60], Mu et al. [61], Manya et al. [62], Harris et al. [63], and Archer and Carter [66] scatter more and show higher deviations from

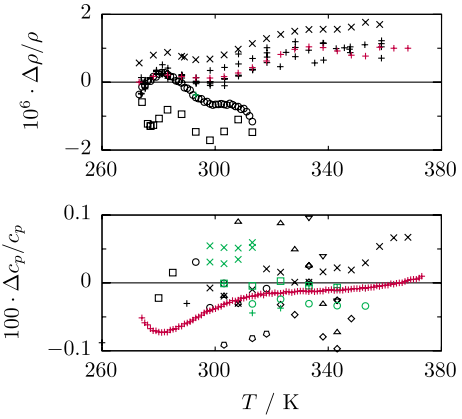

Fig. 6 Relative deviations of the initial values of the thermodynamic integration for the density and specific isobaric heat capacity and experimental data of other groups from the literature from values calculated with the IAPWS-95 formulation at ambient pressure. Experimental densities: +, initial values; +, Takenaka and Masui [49]; +, Wolf et al. [53]; ○, Tanaka et al. [54]; ×, Masui et al. [52]; □, Patterson and Morris [55]. Experimental isobaric heat capacities: +, Osborne et al. [50]; ▽, He et al. [56]; ○, Gómez-Álvarez et al. [57]; +, Shokouhi et al. [58]; □, Shokouhi et al. [59]; ×, Wasiak et al. [60]; ○, Mu et al. [61]; ◇, Manya et al. [62]; △, Harris et al. [63]; ×, Anouti et al. [64]; ○, García-Miaja et al. [65]; □, Archer and Carter [66]; +, Angell et al. [67]

the IAPWS-95 formulation, which, however, remain mostly within 0.1%. Based on this comparison, we estimate the relative expanded ($k = 2$) uncertainty in the initial values for the isobaric heat capacity to be 0.1%.

The thermodynamic integration was carried out by integrating the partial differential equations, Eqs. 4 and 5, numerically in discrete pressure steps by the predictor-corrector algorithm described by Dávila and Trusler [68]. Starting on the initial isobar, densities and specific isobaric heat capacities at the next higher pressure are calculated by the predictor step

$$\rho(p_1) = \rho(p_0) + \Delta p \left(\frac{\partial \rho}{\partial p} \right)_{T,p_0} \tag{7}$$

and

$$c_p(p_1) = c_p(p_0) + \Delta p \left(\frac{\partial c_p}{\partial p} \right)_{T,p_0}, \tag{8}$$

in which p_0 denotes the initial pressure, Δp the pressure step size of the integration, and $p_1 = p_0 + \Delta p$ the pressure of the next isobar. The partial derivatives $(\partial\rho/\partial p)_T$ and $\left(\partial c_p/\partial p\right)_T$ on the initial isobar are calculated with Eqs. 4 and 5. Values for the derivatives $(\partial\rho/\partial T)_p$ and $\left(\partial^2\rho/\partial T^2\right)_p$ at the initial isobar required in Eqs. 4 and 5 are calculated with the analytical derivatives of Eq. 6 and the polynomials used for interpolation of the initial values of the isobaric heat capacity in Table 6 of Ref. [50]. At each further pressure step, the calculated densities were fitted to

seventh-order polynomials as functions of temperature. With these polynomials, the derivatives $(\partial\rho/\partial T)_p$ and $\left(\partial^2\rho/\partial T^2\right)_p$ for the next integration step were calculated. The equations for the corrector step

$$\rho(p_1) = \rho(p_0) + \frac{1}{2}\Delta p\left[\left(\frac{\partial\rho}{\partial p}\right)_{T,p_0} + \left(\frac{\partial\rho}{\partial p}\right)_{T,p_1}\right] \tag{9}$$

and

$$c_p(p_1) = c_p(p_0) + \frac{1}{2}\Delta p\left[\left(\frac{\partial c_p}{\partial p}\right)_{T,p_0} + \left(\frac{\partial c_p}{\partial p}\right)_{T,p_1}\right] \tag{10}$$

contain the derivatives at both isobars p_0 and p_1 and yield the final values for the density and specific isobaric heat capacity at the pressure p_1. At this point, the calculated densities and isobaric heat capacities at the isobar p_1 serve as initial values for the next integration step. This procedure is repeated until the final pressure is reached.

The integration is carried out on a grid in discrete pressure steps along the isotherm 273.65 K and in the temperature range between 278.15 K and 368.15 K along isotherms in steps of 5 K. This step size was found suitable to stabilize the polynomial fits at each pressure step. The numerical stability of the predictor-corrector method was assessed by performing the integration tentatively with pressure step sizes of 0.01 MPa and 0.1 MPa. Since the differences between the results for the density and isobaric heat capacity with the two step sizes were less than 0.02 ppm in the whole range of the integration, 0.1 MPa was chosen as step size. With this choice, the numerical error of the integration algorithm is negligible. In addition to the density and isobaric heat capacity, values for the isochoric heat capacity were calculated using the results of the thermodynamic integration by the relation

$$c_v = c_p - \frac{T}{\rho^2}\left(\frac{\partial\rho}{\partial T}\right)_p^2\left(\frac{\partial\rho}{\partial p}\right)_T^{-1}. \tag{11}$$

The uncertainties in the derived properties were estimated by propagating the uncertainties in the initial values for the density and isobaric heat capacity and in the speed of sound correlation by the Gaussian error-propagation law through the predictor-corrector algorithm. Details of the application of the Gaussian error-propagation law to the thermodynamic integration can be found in Ref. [69]. We note that Trusler and Lemmon [3] proposed a method for the uncertainty analysis of the thermodynamic integration which takes into account rapid oscillations of the speed of sound correlation and polynomial fits to the initial values resulting from overfitting of the data. Since our speed of sound correlation does not show such oscillations as is evident from Fig. 3 and the initial values for the density and isobaric heat capacity were derived from a highly accurate correlation and accurate tabulated data, we assume that our method in this work is free of this type of error. The relative expanded ($k = 2$) uncertainty in the derived densities is estimated to be 2 ppm in

the whole temperature and pressure range of the integration. The relative expanded ($k = 2$) uncertainty in the isobaric heat capacity increases with pressure at all isotherms, starting with the uncertainty in the initial values of 0.1% at ambient pressure and increasing to 0.11% at 100 MPa. The relative expanded ($k = 2$) uncertainty in the isochoric heat capacity amounts to 0.11% at ambient pressure and increases to 0.12% at 100 MPa. The results of the thermodynamic integration for the density and isobaric and isochoric heat capacities are listed in Table 5.

In the remainder of this section, the derived properties are compared with the IAPWS-95 formulation [5], experimental data for the density and isobaric and isochoric heat capacities of other authors from the literature, and values obtained by Trusler and Lemmon [3] by thermodynamic integration of the speed of sound data of Lin and Trusler [4]. In this discussion, we use the uncertainties assigned by Wagner and Pruß [5] and Wagner and Thol [70] to experimental data used in the development of the IAPWS-95 formulation and assume that they are expanded ($k = 2$) uncertainties.

The distribution of the experimental data for the density is shown in a pressure–temperature diagram in Fig. 7. Among the numerous data sets for the density of water at high pressure [5] to which the IAPWS-95 formulation was fitted only those of Tammann and Jellinghaus [71], Bridgman [72], Grindley and Lind [73], Kell and Whalley [74], Kell et al. [75], and Hilbert et al. [76] cover the range of low temperature. Bridgman [72] and Tammann and Jellinghaus [71] measured the density in the high pressure region of the pressure–temperature diagram, in which water is liquid below 273.15 K. These data sets do not overlap with the region of our thermodynamic integration. The data of Kell and Whalley [74] cover the range of our thermodynamic integration completely, and they are with a relative expanded ($k = 2$) uncertainty of 10 ppm to 30 ppm the most accurate data for the density of water at high pressure. The data of Grindley and Lind, Kell et al., and Hilbert et al. overlap only partially with the region of our thermodynamic integration or the thermodynamic integration of Trusler and Lemmon and have larger relative expanded ($k = 2$) uncertainties of 0.01% to 0.05%, 0.01% to 0.02%, and 0.2%, respectively, than the data of Kell and Whalley. Therefore, only the data of Kell and Whalley were selected for the discussion. Lin and Trusler [4] measured the speed of sound in liquid water between 253.15 K and 473.15 K up to 400 MPa and derived thermodynamic properties from their measurements by the method of thermodynamic integration. Recently, Trusler and Lemmon [3] improved the results of Lin and Trusler by repeating the thermodynamic integration with a more accurate speed of sound correlation and smaller temperature step size. The results of Trusler and Lemmon are also considered in the discussion. The initial values for the density and isobaric heat capacity for their thermodynamic integration were calculated with the IAPWS-95 formulation.

Figure 8 depicts relative deviations of our derived densities, experimental data from the literature at nearby temperatures, densities derived by Trusler and Lemmon [3] from the speed of sound measurements of Lin and Trusler [4], and the equation of state of Holten et al. [29] from the IAPWS-95 formulation. Our derived densities agree with the IAPWS-95 formulation within 10 ppm at all isotherms except for 273.65 K, where the data above 40 MPa deviate by up 30 ppm from the formulation, and 283.15 K and 293.15 K, where the deviations increase up to −15 ppm

Table 5 Values of the density ρ, the specific isobaric heat capacity c_p, and the specific isochoric heat capacity c_v of liquid water determined by thermodynamic integration as a function of temperature T and pressure p. p_{amb} has the value 101.325 kPa

p	ρ	c_p	c_v	ρ	c_p	c_v
MPa	kg · m^{-3}	kJ · (kg · K)$^{-1}$	kJ · (kg · K)$^{-1}$	kg · m^{-3}	kJ · (kg · K)$^{-1}$	kJ · (kg · K)$^{-1}$
	T = 273.65 K			T = 283.15 K		
p_{amb}	999.8729	4.21558	4.21373	999.7011	4.19218	4.18761
5	1002.343	4.19242	4.19153	1002.030	4.17395	4.16801
10	1004.836	4.16996	4.16969	1004.383	4.15615	4.14865
15	1007.301	4.14867	4.14866	1006.710	4.13914	4.12993
20	1009.739	4.12849	4.12840	1009.013	4.12289	4.11182
25	1012.149	4.10937	4.10889	1011.292	4.10738	4.09429
30	1014.532	4.09127	4.09009	1013.546	4.09257	4.07734
35	1016.888	4.07414	4.07199	1015.776	4.07844	4.06093
40	1019.217	4.05794	4.05455	1017.983	4.06496	4.04506
45	1021.519	4.04262	4.03774	1020.167	4.05210	4.02970
50	1023.795	4.02813	4.02154	1022.327	4.03983	4.01484
55	1026.045	4.01444	4.00593	1024.465	4.02812	4.00045
60	1028.270	4.00151	3.99088	1026.580	4.01696	3.98652
65	1030.469	3.98928	3.97637	1028.673	4.00632	3.97303
70	1032.643	3.97772	3.96237	1030.745	3.99617	3.95997
75	1034.793	3.96680	3.94887	1032.795	3.98649	3.94731
80	1036.918	3.95647	3.93583	1034.824	3.97726	3.93505
85	1039.020	3.94671	3.92324	1036.833	3.96845	3.92317
90	1041.099	3.93747	3.91107	1038.821	3.96006	3.91165
95	1043.155	3.92873	3.89931	1040.789	3.95204	3.90048
100	1045.188	3.92045	3.88793	1042.738	3.94440	3.88964
	T = 293.15 K			T = 303.15 K		
p_{amb}	998.2056	4.18185	4.15446	995.6480	4.17851	4.11593
5	1000.438	4.16682	4.13721	997.8205	4.16543	4.10056
10	1002.694	4.15207	4.12010	1000.015	4.15253	4.08529
15	1004.926	4.13789	4.10349	1002.187	4.14007	4.07040
20	1007.135	4.12425	4.08736	1004.336	4.12804	4.05591
25	1009.321	4.11115	4.07169	1006.464	4.11643	4.04179
30	1011.485	4.09855	4.05647	1008.570	4.10521	4.02804
35	1013.627	4.08645	4.04170	1010.655	4.09438	4.01465
40	1015.747	4.07483	4.02734	1012.719	4.08392	4.00161
45	1017.846	4.06366	4.01340	1014.763	4.07383	3.98890
50	1019.924	4.05292	3.99985	1016.787	4.06408	3.97652
55	1021.981	4.04262	3.98669	1018.791	4.05466	3.96445
60	1024.018	4.03271	3.97390	1020.775	4.04557	3.95270
65	1026.034	4.02320	3.96148	1022.741	4.03680	3.94125
70	1028.031	4.01406	3.94940	1024.687	4.02832	3.93008
75	1030.009	4.00528	3.93766	1026.616	4.02014	3.91920
80	1031.967	3.99685	3.92624	1028.526	4.01223	3.90860

Table 5 (continued)

p	ρ	c_p	c_v	ρ	c_p	c_v
MPa	kg · m^{-3}	kJ · (kg · K)$^{-1}$	kJ · (kg · K)$^{-1}$	kg · m^{-3}	kJ · (kg · K)$^{-1}$	kJ · (kg · K)$^{-1}$
85	1033.906	3.98875	3.91515	1030.419	4.00460	3.89826
90	1035.827	3.98097	3.90435	1032.294	3.99723	3.88818
95	1037.729	3.97349	3.89386	1034.152	3.99011	3.87835
100	1039.614	3.96631	3.88365	1035.993	3.98323	3.86877
	$T = 313.15$ K			$T = 323.15$ K		
p_{amb}	992.2153	4.17862	4.07265	988.0343	4.18074	4.02558
5	994.3543	4.16673	4.05886	990.1607	4.16959	4.01317
10	996.5146	4.15497	4.04511	992.3076	4.15853	4.00077
15	998.6521	4.14357	4.03169	994.4313	4.14779	3.98864
20	1000.767	4.13253	4.01859	996.5322	4.13737	3.97677
25	1002.861	4.12184	4.00580	998.6110	4.12725	3.96517
30	1004.933	4.11148	3.99331	1000.668	4.11742	3.95381
35	1006.985	4.10144	3.98112	1002.704	4.10787	3.94271
40	1009.015	4.09171	3.96922	1004.719	4.09860	3.93184
45	1011.026	4.08229	3.95760	1006.714	4.08959	3.92122
50	1013.017	4.07316	3.94626	1008.689	4.08084	3.91082
55	1014.988	4.06431	3.93518	1010.645	4.07234	3.90065
60	1016.941	4.05573	3.92436	1012.581	4.06408	3.89069
65	1018.875	4.04742	3.91380	1014.499	4.05605	3.88096
70	1020.791	4.03937	3.90348	1016.399	4.04825	3.87143
75	1022.689	4.03156	3.89340	1018.281	4.04067	3.86211
80	1024.569	4.02399	3.88356	1020.145	4.03330	3.85298
85	1026.432	4.01665	3.87394	1021.993	4.02613	3.84405
90	1028.278	4.00953	3.86454	1023.823	4.01917	3.83531
95	1030.107	4.00263	3.85536	1025.637	4.01239	3.82676
100	1031.920	3.99594	3.84639	1027.435	4.00581	3.81839
	$T = 333.15$ K			$T = 343.15$ K		
p_{amb}	983.1952	4.18442	3.97592	977.7640	4.18963	3.92468
5	985.3262	4.17370	3.96473	979.9143	4.17908	3.91457
10	987.4767	4.16305	3.95353	982.0831	4.16861	3.90444
15	989.6030	4.15271	3.94256	984.2264	4.15843	3.89450
20	991.7058	4.14265	3.93181	986.3448	4.14852	3.88475
25	993.7856	4.13286	3.92128	988.4390	4.13888	3.87517
30	995.8429	4.12335	3.91095	990.5098	4.12950	3.86578
35	997.8785	4.11409	3.90084	992.5578	4.12037	3.85657
40	999.8927	4.10508	3.89093	994.5835	4.11148	3.84752
45	1001.886	4.09632	3.88121	996.5875	4.10281	3.83865
50	1003.859	4.08779	3.87169	998.5704	4.09438	3.82995
55	1005.812	4.07949	3.86237	1000.533	4.08616	3.82140
60	1007.746	4.07140	3.85323	1002.475	4.07815	3.81302
65	1009.661	4.06354	3.84427	1004.398	4.07035	3.80480

Table 5 (continued)

p	ρ	c_p	c_v	ρ	c_p	c_v
MPa	kg · m^{-3}	kJ · (kg · K)$^{-1}$	kJ · (kg · K)$^{-1}$	kg · m^{-3}	kJ · (kg · K)$^{-1}$	kJ · (kg · K)$^{-1}$
70	1011.557	4.05588	3.83549	1006.301	4.06274	3.79673
75	1013.435	4.04842	3.82688	1008.186	4.05532	3.78881
80	1015.296	4.04115	3.81845	1010.052	4.04809	3.78105
85	1017.139	4.03408	3.81019	1011.901	4.04104	3.77342
90	1018.965	4.02719	3.80209	1013.732	4.03416	3.76594
95	1020.774	4.02047	3.79415	1015.546	4.02745	3.75860
100	1022.567	4.01393	3.78637	1017.344	4.02091	3.75140
	$T = 353.15$ K			$T = 363.15$ K		
p_{amb}	971.7899	4.19647	3.87254	965.3088	4.20513	3.82011
5	973.9729	4.18586	3.86337	967.5369	4.19434	3.81182
10	976.1731	4.17534	3.85418	969.7809	4.18363	3.80349
15	978.3460	4.16512	3.84515	971.9955	4.17321	3.79530
20	980.4925	4.15517	3.83628	974.1815	4.16309	3.78723
25	982.6133	4.14550	3.82757	976.3401	4.15323	3.77929
30	984.7092	4.13608	3.81901	978.4719	4.14364	3.77149
35	986.7809	4.12692	3.81061	980.5779	4.13430	3.76381
40	988.8291	4.11799	3.80235	982.6589	4.12521	3.75627
45	990.8545	4.10930	3.79425	984.7156	4.11636	3.74885
50	992.8577	4.10084	3.78629	986.7487	4.10773	3.74156
55	994.8393	4.09259	3.77847	988.7589	4.09932	3.73439
60	996.7998	4.08455	3.77080	990.7468	4.09113	3.72735
65	998.7399	4.07671	3.76326	992.7132	4.08314	3.72042
70	1000.660	4.06906	3.75586	994.6584	4.07536	3.71362
75	1002.561	4.06161	3.74859	996.5832	4.06776	3.70693
80	1004.442	4.05434	3.74144	998.4880	4.06035	3.70036
85	1006.305	4.04724	3.73443	1000.373	4.05312	3.69389
90	1008.150	4.04032	3.72754	1002.240	4.04607	3.68753
95	1009.977	4.03356	3.72077	1004.088	4.03918	3.68128
100	1011.787	4.02696	3.71411	1005.917	4.03246	3.67513
	$T = 368.15$ K					
p_{amb}	961.8862	4.21028	3.79424			
5	964.1413	4.19942	3.78640			
10	966.4117	4.18863	3.77850			
15	968.6513	4.17813	3.77070			
20	970.8613	4.16790	3.76301			
25	973.0427	4.15794	3.75544			
30	975.1964	4.14823	3.74798			
35	977.3233	4.13878	3.74063			
40	979.4243	4.12956	3.73340			
45	981.5002	4.12058	3.72629			
50	983.5517	4.11182	3.71929			

Table 5 (continued)

p MPa	ρ kg · m^{-3}	c_p kJ · (kg · K)$^{-1}$	c_v kJ · (kg · K)$^{-1}$	ρ kg · m^{-3}	c_p kJ · (kg · K)$^{-1}$	c_v kJ · (kg · K)$^{-1}$
55	985.5796	4.10329	3.71240			
60	987.5845	4.09496	3.70563			
65	989.5671	4.08685	3.69897			
70	991.5280	4.07894	3.69243			
75	993.4679	4.07122	3.68599			
80	995.3872	4.06369	3.67966			
85	997.2865	4.05634	3.67344			
90	999.1663	4.04918	3.66733			
95	1001.027	4.04219	3.66132			
100	1002.869	4.03537	3.65540			

Relative expanded ($k = 2$) uncertainties: $U_r(\rho) = 2$ ppm, $U_r(c_p) = 0.11\%$, and $U_r(c_v) = 0.12\%$

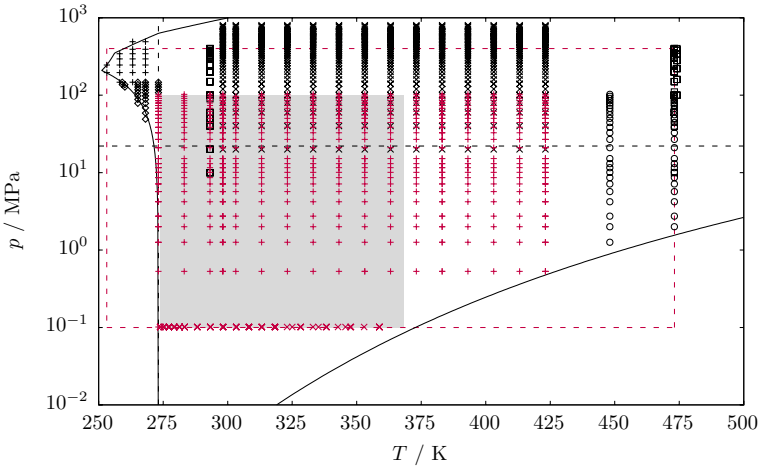

Fig. 7 Distribution of data for the density of water of other authors from the literature in a pressure–temperature diagram. The gray shaded region denotes the region of our thermodynamic integration. The red dotted rectangle indicates the region of thermodynamic integration of Trusler and Lemmon [3]. Experimental data: ×, Takenaka and Masui [49]; □, Hilbert et al. [76]; ○, Kell et al. [75]; +, Kell and Whalley [74]; ×, Grindley and Lind [73]; +, Bridgman [72]; ◇, Tammann and Jellinghaus [71]; - - - -, critical pressure and triple point temperature; ——, vapor and melting pressure curves calculated with the IAPWS-95 formulation and the reference equation for the melting pressure of Wagner et al. [27], respectively

and −13 ppm near 100 MPa, respectively. At the isotherms 343.15 K and 353.15 K, the deviations remain even within 5 ppm. The data of Kell and Whalley exhibit the same pressure dependence as our derived densities at the isotherms at 273.65 K, 283.15 K, 303.15 K, 313.15 K, and 333.15 K, but show some scatter in the high resolution of the deviation plots. On the other isotherms, they show a different pressure dependence than our derived densities, and especially at pressures below 60 MPa

the deviations from our values increase up to −20 ppm. The derived densities of Trusler and Lemmon also show the same pressure dependence as our derived values on most isotherms, but also show some scatter and the initial values at ambient pressure deviate systematically by up to between −16 ppm and +19 ppm from the data of Takenaka and Masui and the IAPWS-95 formulation, although they were calculated with the formulation. These systematic deviations and the scatter of the data are due to round-off errors in the data of Trusler and Lemmon. They reported density values with only five respectively six figures, which is not sufficient to achieve parts-per-million accuracy.

The EOS of Holten et al. [29] agrees with our derived densities within 5 ppm on the four isotherms between 273.65 K and 303.15 K. Up to 40 MPa, the deviations remain within the uncertainty of our data of 1 ppm, while at higher pressures the deviations are larger. The largest deviation of −5 ppm is observed at 303.15 K and 100 MPa. We note that the isotherm 303.15 K is slightly above the upper limit of validity of 300 K of the Holten et al. EOS. Holten et al. estimated the relative expanded ($k = 2$) uncertainty in densities calculated with their EOS to between 10 ppm to 30 ppm. Thus, our derived densities agree with the Holten et al. EOS within much less than its uncertainty, which indicates that the uncertainty estimates for the EOS are too conservative.

The distribution of data for the isobaric heat capacity of water of other authors from the literature is depicted in Fig. 9. The data of Sirota et al. [82] with a relative expanded ($k = 2$) uncertainty of 0.3% are the most accurate experimental data for the isobaric heat capacity of water. Several other data sets overlap partially with the range of the thermodynamic integration, e.g., the data of Troncoso [77], Zheng et al. [78], Zhao et al. [79], Ernst and Philippi [80], and Naziev et al. [81]. However, most of these data scatter more than the data of Sirota et al. [82] and have larger uncertainties than our derived isobaric heat capacities. For example, Troncoso [77] published 3050 data points at high pressures between 100 MPa and 500 MPa, which scatter within ±1%. Gómez-Álvarez et al. [57] reported a rather high uncertainty of their data of 2%, but, as will be discussed below, their data agree well with the IAPWS-95 formulation. Thus, only the data of Sirota et al. [82] and Gómez-Álvarez et al. [57] and the derived isobaric heat capacities of Trusler and Lemmon [3] are considered in the comparison.

Figure 10 depicts relative deviations of our derived isobaric heat capacities, the experimental data of Osborne et al. [50], Gomez-Alvarez et al. [57], Zheng et al. [78], and Sirota et al. [82], the derived isobaric heat capacities of Trusler and Lemmon [3], and isobaric heat capacities calculated with the Holten et al. EOS [29] at nearby temperatures from the IAPWS-95 formulation. In the region of our thermodynamic integration, the relative expanded ($k = 2$) uncertainty in the IAPWS-95 formulation is 0.1% up to 20 MPa and 0.3% at higher pressures up to 100 MPa below 300 K and 0.1% up to 60 MPa and 0.3% at higher pressures up to 100 MPa above 300 K. Our derived isobaric heat capacities agree with the IAPWS-95 formulation mostly within its uncertainty on all isotherms. Only at 273.65 K and high pressures, the deviations exceed the uncertainty of the IAPWS-95 formulation slightly and reach 0.35% at 100 MPa. Nevertheless, the agreement is within the mutual uncertainties. The deviations from the IAPWS-95 formulation decrease with

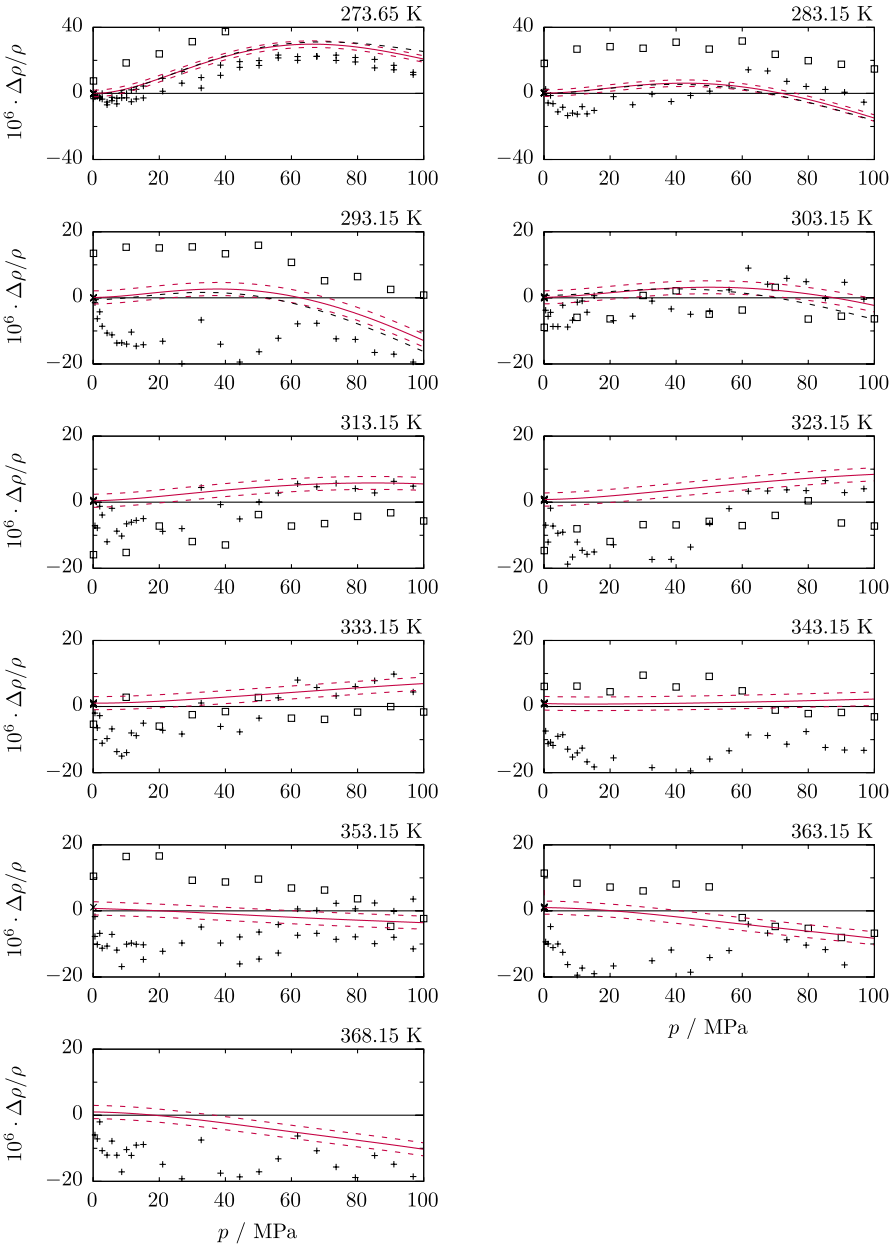

Fig. 8 Relative deviations of our derived densities, derived densities of Trusler and Lemmon, experimental data of Kell and Whalley, and values calculated with the EOS of Holten et al. [29] from values calculated with the IAPWS-95 formulation as a function of pressure. Thermodynamic integration: ——, this work; - - - -, estimated uncertainty range; □, Trusler and Lemmon [3]. Experimental data: ×, Takenaka and Masui [49] and +, Kell and Whalley [74]. - - - -, EOS of Holten et al. [29]

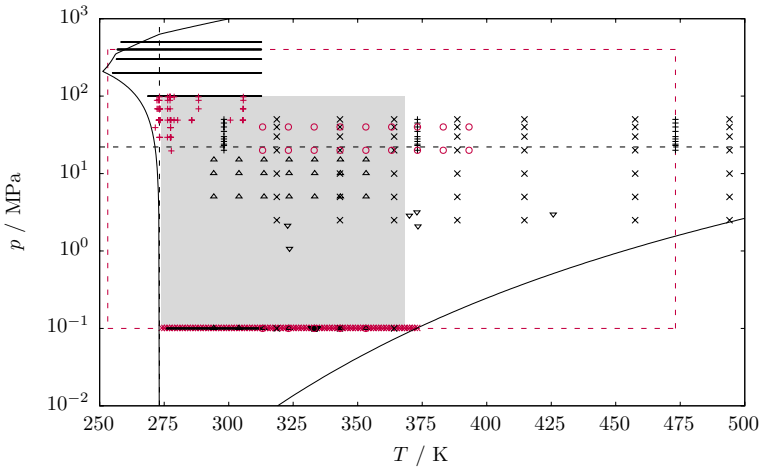

Fig. 9 Distribution of experimental data for the isobaric heat capacity of water of other authors from the literature in a pressure–temperature diagram. The gray shaded region denotes the region of our thermodynamic integration. The red dotted rectangle indicates the region of thermodynamic integration of Trusler and Lemmon [3]. Experimental data: ×, Osborne et al. [50]; ○, Gómez-Álvarez et al. [57]; ·, Troncoso [77]; △, Zheng et al. [78]; ▽, Zhao et al. [79]; +, Ernst and Philippi [80]; ×, Naziev et al. [81]; and + , Sirota et al. [82]. - - - -, critical pressure and triple point temperature. ——, vapor and melting pressure curves calculated with the IAPWS-95 formulation and the reference equation for the melting pressure of Wagner et al. [27], respectively

increasing temperature, reaching 0.03% at 303.15 K and 0.01% between 343.15 K and 368.15 K.

The data of Sirota et al. [82] have a relative expanded ($k = 2$) uncertainty of 0.3% and show some scatter. On the isotherm 273.15 K, they show a similar pressure dependence as our derived values and agree with them mostly within the mutual uncertainties. At the higher isotherms 283.15 K, 293.15 K, and 303.15 K, the agreement with our values is within 0.2%. Gómez-Álvarez et al. [57] measured the isobaric heat capacity of water between 313.15 K and 393.15 K in steps of 10 K at 0.1 MPa, 20 MPa, and 40 MPa. Their data agree with our derived isobaric heat capacities within 0.02%. This close agreement is remarkable since the uncertainty of their data of 2% is much higher.

The derived isobaric heat capacities of Trusler and Lemmon [3] lie inside the uncertainty of our values on all isotherms except at 273.65 K at high pressures above 50 MPa, where they deviate from our values by 0.15%. Since Trusler and Lemmon [3] did not use the data of Osborne et al. [50] as initial values for their thermodynamic integration, but calculated the initial values with the IAPWS-95 formulation, deviations up to 0.05% from our results at ambient pressure are found, which are propagated by the thermodynamic integration with increasing pressure. Wagner and Thol [70] derived estimates of the relative expanded ($k = 2$) uncertainty in the derived isobaric heat capacities of Trusler and Lemmon by comparing the derived values with the EOS of Holten et al. [29]. They obtained 0.05% at ambient pressure and 0.17% between 1 MPa and 400 MPa. Thus, the derived values of Trusler and Lemmon agree with our values within their uncertainty. As the derived density data

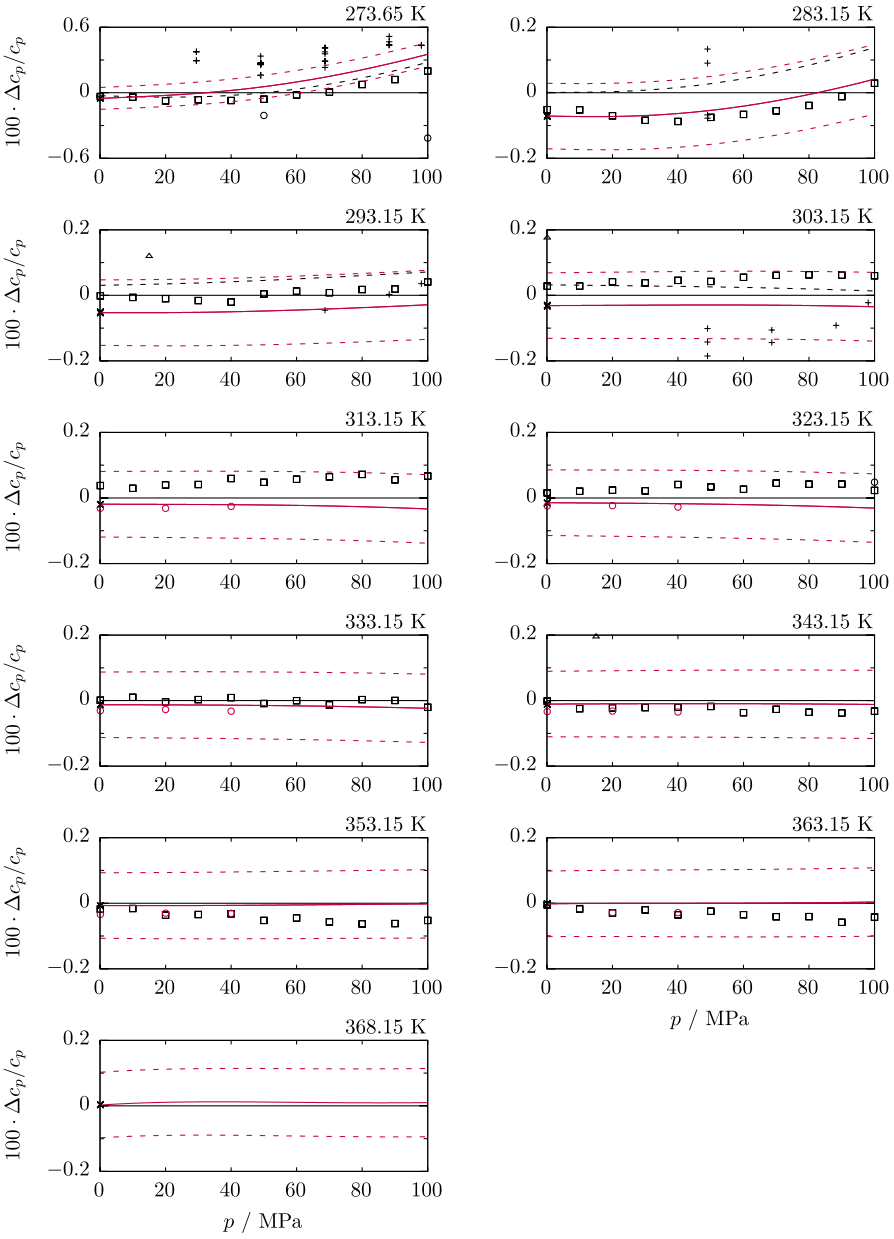

Fig. 10 Relative deviations of our derived isobaric heat capacities and data of other authors from the literature from values calculated with the IAPWS-95 formulation as a function of pressure. Thermodynamic integration: ——, this work; - - - -, estimated uncertainty range. □, Trusler and Lemmon [3]. Experimental data: ×, Osborne et al. [50]; ○, Gomez-Alvarez et al. [57]; △, Zheng et al. [78]; and +, Sirota et al. [82]. - - - -, EOS of Holten et al. [29]

of Trusler and Lemmon, the derived isobaric heat capacities also show some scatter because they are reported with only four figures. The Holten et al. EOS [29] agrees with our derived isobaric heat capacities within the uncertainty of our values and confirms them between 273.65 K and 303.15 K.

Figure 11 shows the distribution of experimental data for the isochoric heat capacity of water of other authors from the literature in a pressure–temperature diagram. The most comprehensive data sets of Kuroki et al. [83], Magee et al. [84], and Abdulagatov et al. [85] partially overlap with the region of the thermodynamic integration. Kuroki et al. performed measurements between 316.2 K and 365.2 K at pressures between 2 MPa and 20 MPa with a relative expanded ($k = 2$) uncertainty of 1%. The data of Magee et al. cover the liquid region between 304 K and 413 K with pressures up to 20 MPa. Their data have a relative expanded ($k = 2$) uncertainty of 0.3%. Abdulagatov et al. measured the liquid region between 321 K and 576 K at pressures between 0.9 MPa and 12 MPa with a relative expanded ($k = 2$) uncertainty of 0.8%. Trusler and Lemmon [3] published values for the isobaric thermal expansivity $\alpha_p = -\rho^{-1}(\partial\rho/\partial T)_p$ and the isothermal compressibility $\kappa_T = -\rho^{-1}(\partial\rho/\partial p)_T$ obtained from their thermodynamic integration, which we used together with their values for the isobaric heat capacity to calculate isochoric heat capacities by using Eq. 11. These values for the isochoric heat capacity are also included in the following comparison and are referred to as the derived values of Trusler and Lemmon.

Figure 12 depicts relative deviations of our derived isochoric heat capacities, the experimental data of Kuroki et al. [83], Magee et al. [84], the derived isochoric heat capacities of Trusler and Lemmon [3], and isochoric heat capacities calculated with the Holten et al. EOS [29] from the IAPWS-95 formulation. Our derived isochoric heat capacities agree with the IAPWS-95 formulation within 0.3% or less on all isotherms. Again, the largest deviations are observed at 273.65 K and 100 MPa. The agreement with the IAPWS-95 formulation becomes better with increasing temperature and is best at the highest isotherms. The pressure dependence of the deviations is similar to that of our derived isobaric heat capacities in Fig. 10. The data of Kuroki et al. [83] and Magee et al. [84] deviate by up to 1% and 0.8%, respectively, from the IAPWS-95 formulation and lie only partially inside the scale of the plots.

The derived values of Trusler and Lemmon [3] agree with our derived values mostly within the uncertainty of our values. Only at 273.65 K above 50 MPa, their results lie outside the uncertainty margin of our values as already observed for the isobaric heat capacity. The derived values of Trusler and Lemmon [3] show some scatter due to round-off errors in their reported values for the isobaric thermal expansivity and isothermal compressibility as their derived values for the density and isobaric heat capacity. The EOS of Holten et al. [29] agrees with our values within our estimated uncertainty and shows the same pressure dependence as our values, which provides a further confirmation of the high accuracy of the results of the thermodynamic integration.

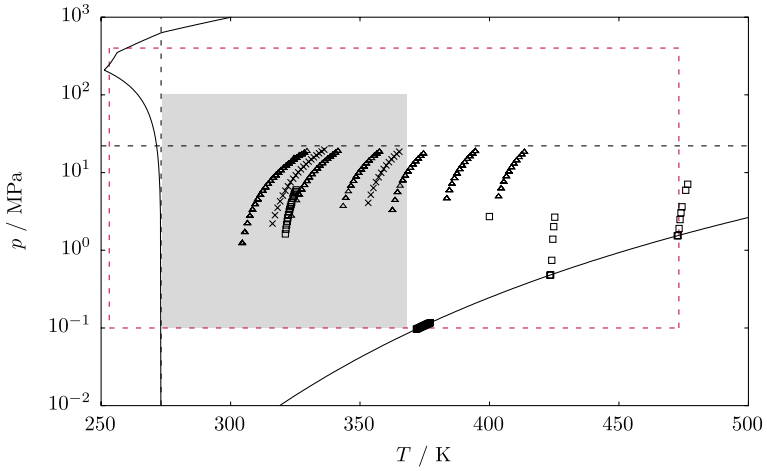

Fig. 11 Distribution of data for the isochoric heat capacity of water of other authors from the literature in a pressure–temperature diagram. The gray shaded region denotes the region of our thermodynamic integration. The red dotted rectangle encircles the region of thermodynamic integration of Trusler and Lemmon [3]. Experimental data: ×, Kuroki et al. [83]; △, Magee et al. [84]; and □, Abdulagatov et al. [85]. - - - -, critical pressure and triple point temperature. ——, vapor and melting pressure curves calculated with the IAPWS-95 formulation and the reference equation for the melting pressure of Wagner et al. [27], respectively

5 Conclusions

Accurate measurements of the speed of sound in liquid water were carried out in the temperature range between 273.65 K and 368.15 K with pressures up to 100 MPa with low expanded ($k = 2$) uncertainties between 40 ppm and 70 ppm. By the method of thermodynamic integration, thermodynamically consistent and accurate values for the density, isobaric heat capacity, and isochoric heat capacity were calculated in the measured temperature and pressure range. Especially, the results for the density have a very low expanded ($k = 2$) uncertainty of only 2 ppm. In contrast to previous works of other authors, we derived the initial values for the density and isobaric heat capacity from the most accurate experimental for these properties at ambient pressure. Thus, our results were obtained independently of the IAPWS-95 formulation. Our speed of sound data agree well with the most accurate experimental speed of sound data of other authors from the literature and the EOS of Holten et al. [29]. Moreover, we find good agreement of our derived properties with experimental data of other authors from the literature and with recent values obtained by means of the thermodynamic integration from speed of sound data by Trusler and Lemmon [3]. Generally, our results agree with the IAPWS-95 formulation within its uncertainty with the exception of a small region at low temperature and high pressure, but they have smaller uncertainties

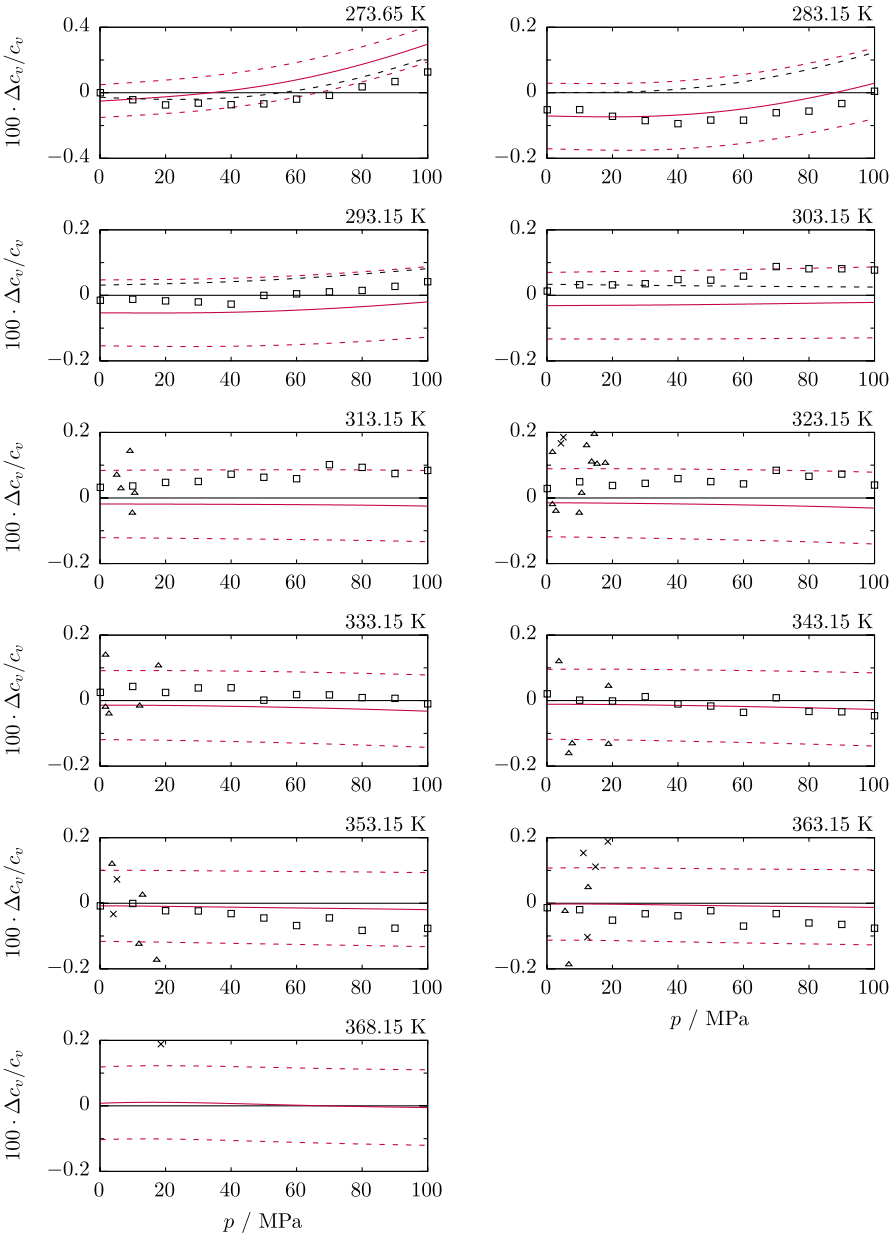

Fig. 12 Relative deviations of our derived values for the isochoric heat capacity of water and data of other authors from the literature from values calculated with the IAPWS-95 formulation as a function of pressure. Thermodynamic integration: ——, this work; - - - -, estimated uncertainty range; □, Trusler and Lemmon [3]. Experimental data: ×, Kuroki et al. [83]; and △, Magee et al. [84]. - - - -, EOS of Holten et al. [29]

than the IAPWS-95 formulation. The results for the derived properties show that very accurate data for thermodynamic properties can be derived from speed of sound data sets by thermodynamic integration if very accurate data for the initial conditions are available.

The new speed of sound data and the results for the density and isobaric and isochoric heat capacities of the thermodynamic integration can contribute to the development of a new more accurate formulation for the thermodynamic properties of water which succeeds the IAPWS-95 formulation in the future. The results for the density and isobaric and isochoric heat capacities can either directly be used in the fitting process of a new formulation or serve as data for validating a new formulation if they are not included in the fitting process. Moreover, the derived values for the density data can be applied as references in the calibration of vibrating-tube densimeters, for which water is often employed as a calibration fluid. Thus, the low uncertainty of the derived values contributes to reducing the uncertainty in density measurements with vibrating-tube densimeters.

However, the highly accurate density data that were determined in this work from measured speed of sound data suggest at the same time that density measurements may not be needed in the future to the same extent as they were until highly accurate speed of sound measurements were established. With acoustic metrology, highly accurate density and heat capacity values are needed only in limited ranges as initial conditions for the thermodynamic integration. Therefore, it appears advantageous in terms of measurement effort and accuracy of experimental results to shift the emphasis of the determination of thermodynamic properties in wide ranges of pressure and temperature henceforth to primary measurements of the speed of sound with supplementary density measurements and heat capacity determinations to enable thermodynamic integration. Thus, all thermodynamic properties can be determined in the same pressure and temperature range while the experimental effort has to be mounted largely for only one property, the speed of sound. This will be a significant advance towards more economical metrology of thermodynamic properties at substantially lower uncertainties.

Acknowledgements We thank our students Jochen Lofink and Jonas Schoepke for their assistance during the measurement campaign. We acknowledge Simona Lago of INRiM in Torino for providing experimental data for the speed of sound in water prior to publication. We also thank Dr. Arno Laesecke, retired from NIST Boulder, for carefully reading the manuscript and valuable suggestions. All IAPWS-95 calculations in this work were carried out with the NIST Standard Reference Database 23 Refprop [86].

Author Contributions AEH performed the measurements and prepared the figures and tables. KM initiated the research project, carried out the evaluation of the literature data, and wrote the manuscript text. All authors reviewed the manuscript.

Funding Open Access funding enabled and organized by Projekt DEAL.

Declarations

Conflict of interest The authors declare no competing interests.

References

1. A. El Hawary, K. Meier, Speed of sound measurements and derived thermodynamic properties of liquid isobutane. J. Chem. Eng. Data **63**, 3684–3703 (2018). https://doi.org/10.1021/acs.jced.8b00202
2. A. El Hawary, K. Meier, Thermodynamic properties of liquid toluene and *n*-butane determined from speed of sound data. Int. J. Thermophys. **43**, 71 (2022). https://doi.org/10.1007/s10765-021-02958-y
3. J.P.M. Trusler, E.W. Lemmon, Determination of the thermodynamic properties of water from the speed of sound. J. Chem. Thermodyn. **109**, 61–70 (2017). https://doi.org/10.1016/j.jct.2016.10.028
4. C.-W. Lin, J.P.M. Trusler, The speed of sound and derived thermodynamic properties of pure water at temperatures between (253 and 473) K and at pressures up to 400 MPa. J. Chem. Phys. **136**, 094511 (2012). https://doi.org/10.1063/1.3688054
5. W. Wagner, A. Pruß, The IAPWS formulation 1995 for the thermodynamic properties of ordinary water substance for general and scientific use. J. Phys. Chem. Ref. Data **31**, 387–535 (2002). https://doi.org/10.1063/1.1461829
6. K. Meier, The pulse-echo method for high precision measurements of the speed of sound in fluids. Postdoctoral thesis, Helmut-Schmidt-Universität/Universität der Bundeswehr Hamburg, Hamburg (2006)
7. K. Meier, S. Kabelac, Speed of sound instrument for fluids with pressures up to 100 MPa. Rev. Sci. Instrum. **77**, 123903 (2006). https://doi.org/10.1063/1.2400019
8. ASTM Committee D19. ASTM Standard D1193-99e1, Standard specification for reagent water, ASTM International, West Conshohocken, PA (1999)
9. R. Gonfiantini, Standards for stable isotope measurements in natural compounds. Nature **271**, 534–536 (1978). https://doi.org/10.1038/271534a0
10. V.A. Del Grosso, C.W. Mader, Speed of sound in pure water. J. Acoust. Soc. Am. **52**, 1442–1446 (1972). https://doi.org/10.1121/1.1913258
11. K. Fujii, *Accurate measurements of the sound velocity in pure water under high pressure* (Personal communication, 1994)
12. W. Kroebel, K.-H. Mahrt, Recent results of absolute sound velocity measurements in pure water and sea water at atmospheric pressure. Acustica **35**, 154–164 (1976)
13. W. Marczak, Water as a standard in the measurements of speed of sound in liquids. J. Acoust. Soc. Am. **102**, 2776–2779 (1997). https://doi.org/10.1121/1.420332
14. K. Fujii, R. Masui, Accurate measurements of the sound velocity in pure water by combining a coherent phase-detection technique and a variable path-length interferometer. J. Acoust. Soc. Am. **93**, 276–282 (1993). https://doi.org/10.1121/1.405661
15. A.A. Aleksandrov, A.I. Kochetov, Experimental determination of ultrasonic velocity in water at temperatures of 266–423 K and pressures up to 100 MPa. Teploenergetika **26**, 65–66 (1979)
16. A.A. Aleksandrov, D.K. Larkin, An experimental determination of the velocity of sound in water within a wide range of temperature and pressure. Teploenergetika **23**, 75–78 (1976)
17. E.H. Baltasar, M. Taravillo, V.G. Baonza, P.D. Sanz, B. Guignon, Speed of sound in liquid water from (253.15 to 348.15) K and pressures from (0.1 to 700) MPa. J. Chem. Eng. Data **56**, 4800–4807 (2011). https://doi.org/10.1021/je200668a
18. A.J. Barlow, E. Yazgan, Pressure dependence of the velocity of sound in water as a function of temperature. Br. J. Appl. Phys. **18**, 645–651 (1967). https://doi.org/10.1088/0508-3443/18/5/315

19. G. Benedetto, R.M. Gavioso, P.A. Giuliano Albo, S. Lago, D. Madonna Ripa, R. Spagnolo, Speed of sound in pure water at temperatures between 274 and 394 K and at pressures up to 90 MPa. Int. J. Thermophys. **26**, 1667–1680 (2005). https://doi.org/10.1007/s10765-005-8587-2
20. O. Bollengier, J.M. Brown, G.H. Shaw, Thermodynamics of pure liquid water: sound speed measurements to 700 MPa down to the freezing point, and an equation of state to 2300 MPa from 240 to 500 K. J. Chem. Phys. **151**, 054501 (2019). https://doi.org/10.1063/1.5097179
21. F. Fehres, Schallgeschwindigkeitsmessungen in Seewasser bei hohen Drücken. PTB-Bericht Th-14, Physikalisch-Technische Bundesanstalt, Braunschweig und Berlin (2021)
22. G. Holton, M.P. Hagelberg, S. Kao, W.H. Johnson, Ultrasonic-velocity measurements in water at pressures to 10000 kg/cm^2. J. Acoust. Soc. Am. **43**, 102–107 (1968). https://doi.org/10.1121/1.1910739
23. S. Lago, P.A.G. Albo, M. Bertinetti, Speed of sound measurements in supercooled water at temperatures between (254.65 and 273.15) K and at pressures up to 190 MPa, to be submitted (2023)
24. J.P. Petitet, R. Tufeu, B. Le Neindre, Determination of the thermodynamic properties of water from measurements of the speed of sound in the temperature range 251.15–293.15 K and the pressure range 0.1–350 MPa. Int. J. Thermophys. **4**, 35–50 (1983). https://doi.org/10.1007/BF00504480
25. W.D. Wilson, Speed of sound in distilled water as a function of temperature and pressure. J. Acoust. Soc. Am. **31**, 1067–1072 (1959). https://doi.org/10.1121/1.1907828
26. S. Ye, J. Alliez, B. Lagourette, H. Saint-Guirons, J. Arman, P. Xans, Réalisation d'un dispositif de mesure de la vitesse et de l'atténuation d'ondes ultrasonores dans des liquides sous pression. Rev. Phys. Appl. **25**, 555–565 (1990). https://doi.org/10.1051/rphysap:01990002506055500
27. W. Wagner, T. Riethmann, R. Feistel, A.H. Harvey, New equations for the sublimation pressure and melting pressure of H_2O Ice Ih. J. Phys. Chem. Ref. Data **40**, 043103 (2011). https://doi.org/10.1063/1.3657937
28. W. Wagner, A mathematical-statistical method for establishing thermodynamic equations – demonstrated using the vapor pressure curve of pure fluid substances as an example. Fortschr.-Ber. VDI-Z. Reihe 3, Nr. 39 (1974)
29. V. Holten, J.V. Sengers, M.A. Anisimov, Equation of state for supercooled water at pressures up to 400 MPa. J. Phys. Chem. Ref. Data **43**, 043101 (2014). https://doi.org/10.1063/1.4895593
30. V. Diky, C.D. Muzny, A.Y. Smolyanitsky, A. Bazyleva, R.D. Chirico, J.W. Magee, E. Paulechka, A.F. Kazakov, S.A. Townsend, E.W. Lemmon, M. Frenkel, K.G. Kroenlein, NIST ThermoData Engine Version 10.0, NIST Standard Reference Database 103b, Standard Reference Data Program, National Institute of Standards and Technology, Gaithersburg, MD (2015)
31. International Association for the Properties of Water and Steam. IAPWS R6-95(2018), Revised release on the IAPWS Formulation 1995 for the thermodynamic properties of ordinary water substance for general and scientific use (2018). http://iapws.org/relguide/IAPWS95-2018.pdf
32. International Association for the Properties of Water and Steam. IAPWS G12-15, Guideline on thermodynamic properties of supercooled water (2015). http://iapws.org/relguide/Supercooled.pdf
33. A.A. Aleksandrov, A.I. Kochetkov, The investigation of sound velocity in water at high pressures, in *Water and Steam—Their Properties and Current Industrial Applications: Proceedings of the 9th International Conference on the Properties of Water and Steam*. ed. by J. Straub, K. Scheffler (Pergamon Press, München, 1979), p. 221
34. N.F. Erokhin, B.I. Kal'yanov, Experimental investigation of the velocity of ultrasound in the critical region of water. High Temp. **17**, 245–251 (1979)
35. V.N. Evstefeev, V.P. Skripov, V.N. Chukanov, Experimental determination of ultrasonic velocity in superheated light and heavy water. High Temp. **17**, 252–257 (1979)
36. N.F. Erokhin, B.I. Kal'yanov, Extremal behavior of ultrasonic velocity and of some other quantities in the supercritical region of water. Teploenergetika **27**, 50–52 (1980)
37. J.P. Petitet, L. Denielou, R. Tufeu, B. Le Neindre, Velocity of sound in supercritical water up to 700°C and 300 MPa. Int. J. Thermophys. **7**, 1065–1075 (1986). https://doi.org/10.1007/BF00502378
38. A.H. Smith, A.W. Lawson, The velocity of sound in water as a function of temperature and pressure. J. Chem. Phys. **22**, 351–359 (1954). https://doi.org/10.1063/1.1740074
39. P.L.M. Heydemann, J.C. Houck, Self-consistent ultrasonic method for the determination of the equation of state of liquids at very high pressures. J. Appl. Phys. **40**, 1609–1613 (1969). https://doi.org/10.1063/1.1657820

40. S. Wiryana, L.J. Slutsky, J.M. Brown, The equation of state of water to 200°C and 3.5 GPa: model potentials and the experimental pressure scale. Earth Plenat. Sci. Lett. **163**, 123–130 (1998). https://doi.org/10.1016/S0012-821X(98)00180-0
41. E.H. Abramson, J.M. Brown, Equation of state of water based on speeds of sound measured in the diamond-anvil cell. Geochim. Cosmochim. Acta **68**, 1827–1835 (2004). https://doi.org/10.1016/j.gca.2003.10.020
42. C. Sanchez-Valle, D. Mantegazzi, J.D. Bass, E. Reusser, Equation of state, refractive index and polarizability of compressed water to 7 GPa and 673 K. J. Chem. Phys. **138**, 054505 (2013). https://doi.org/10.1063/1.4789359
43. M. Chávez, V. Sosa, R. Tsumura, Speed of sound in saturated pure water. J. Acoust. Soc. Am. **77**, 420–423 (1985). https://doi.org/10.1121/1.391861
44. T.A. Litovitz, E.H. Carnevale, Effect of pressure on sound propagation in water. J. Appl. Phys. **26**, 816–820 (1955). https://doi.org/10.1063/1.1722101
45. V.A. Belogol'skii, S.S. Sekoyan, L.M. Samorukova, S.R. Stefanov, V.I. Levtsov, Pressure dependence of the sound velocity in distilled water. Meas. Tech. **42**, 406–413 (1999). https://doi.org/10.1007/BF02504405
46. S. Vance, J.M. Brown, Sound velocities and thermodynamic properties of water to 700 MPa and −10 to 100 °C. J. Acoust. Soc. Am. **127**, 174–180 (2010). https://doi.org/10.1121/1.3257223
47. H. Gedanitz, M.J. Dávila, E. Baumhögger, R. Span, An apparatus for the determination of speeds of sound in fluids. J. Chem. Thermodyn. **42**, 478–483 (2010). https://doi.org/10.1016/j.jct.2009.11.002
48. J.P.M. Trusler, *Physical Acoustics and the Metrology of Fluids* (Adam Hilger, Bristol, 1991)
49. M. Takenaka, R. Masui, Measurement of the thermal expansion of pure water in the temperature range 0°C-85°C. Metrologia **27**, 165–171 (1990). https://doi.org/10.1088/0026-1394/27/4/001
50. N.S. Osborne, H.F. Stimson, D.C. Ginnings, Measurements of heat capacity and heat of vaporization of water in the range 0° to 100° C. J. Res. Natl. Bur. Stand. **23**, 197–260 (1939)
51. M. Menaché, G. Girard, Concerning the different tables of the thermal expansion of water between 0 and 40 °C. Metrologia **9**, 62–68 (1973). https://doi.org/10.1088/0026-1394/9/2/002
52. R. Masui, K. Fujii, M. Takenaka, Determination of the absolute density of water at 16 °C and 0,101 325 MPa. Metrologia **32**, 333–362 (1995). https://doi.org/10.1088/0026-1394/32/5/1
53. H. Wolf, H. Bettin, A. Gluschko, Water density measurement by a magnetic flotation apparatus. Meas. Sci. Technol. **17**, 2581–2587 (2006). https://doi.org/10.1088/0957-0233/17/10/008
54. M. Tanaka, G. Girard, R. Davis, A. Peuto, N. Bignell, Recommended table for the density of water between 0 °C and 40 °C based on recent experimental reports. Metrologia **38**, 301–309 (2001). https://doi.org/10.1088/0026-1394/38/4/3
55. J.B. Patterson, E.C. Morris, Measurement of absolute water density, 1 °C to 40 °C. Metrologia **31**, 277–288 (1994). https://doi.org/10.1088/0026-1394/31/4/001
56. Y. He, N. Gao, G. Chen, Isobaric specific heat capacity of typical lithium chloride liquid desiccants using scanning calorimetry. J. Chem. Thermodyn. **70**, 81–87 (2014). https://doi.org/10.1016/j.jct.2013.10.028
57. P. Gómez-Álvarez, D. González-Salgado, J.-P. Bazile, D. Bessieres, F. Plantier, Excess second-order thermodynamic derivatives of the {2-propanol+water} system from 313.15 K to 403.15 K up to 140 MPa. Experimental and Monte Carlo simulation study. Fluid Phase Equilibr. **358**, 7–26 (2013). https://doi.org/10.1016/j.fluid.2013.08.007
58. M. Shokouhi, A.H. Jalili, A.H. Mohammadian, M. Hosseini-Jenab, S.S. Nouri, Heat capacity, thermal conductivity and thermal diffusivity of aqueous sulfolane solutions. Thermochim. Acta **560**, 63–70 (2013). https://doi.org/10.1016/j.tca.2013.03.017
59. M. Shokouhi, A.H. Jalili, M. Hosseini-Jenab, M. Vahidi, Thermo-physical properties of aqueous solutions of *N*,*N*-dimethylformamide. J. Mol. Liq. **186**, 142–146 (2013). https://doi.org/10.1016/j.molliq.2013.07.005
60. M. Wasiak, W. Kunz, H. Piekarski, Heat capacities and the two-point scaling analysis of short-chain surfactant solutions. Fluid Phase Equilibr. **358**, 78–82 (2013). https://doi.org/10.1016/j.fluid.2013.08.005
61. Y. Mu, X. Wang, Y. Wang, Z. Sha, Specific heat at constant pressure of aqueous mixtures of steviosides RA40 with methanol measured with DSC. J. Tianjin Univ. Sci. Technol. **27**, 25–28 (2012)
62. J.J. Manyà, M.J. Antal, C.K. Kinoshita, S.M. Masutani, Specific heat capacity of pure water at 4.0 MPa between 298.15 and 465.65 K. Ind. Eng. Chem. Res. **50**, 6470–6484 (2011). https://doi.org/10.1021/ie102462g

63. F. Harris, K.A. Kurnia, M.I.A. Mutalib, T. Murugesan, Heat capacity of sodium aminoacetate solutions before and after CO_2 absorption. J. Chem. Eng. Data **55**, 547–550 (2010). https://doi.org/10.1021/je9002948
64. M. Anouti, M. Caillon-Caravanier, Y. Dridi, J. Jacquemin, C. Hardacre, D. Lemordant, Liquid densities, heat capacities, refractive index and excess quantities for {protic ionic liquids+water} binary system. J. Chem. Thermodyn. **41**, 799–808 (2009). https://doi.org/10.1016/j.jct.2009.01.011
65. G. García-Miaja, J. Troncoso, L. Romaní, Excess enthalpy, density, and heat capacity for binary systems of alkylimidazolium-based ionic liquids+water. J. Chem. Thermodyn. **41**, 161–166 (2009). https://doi.org/10.1016/j.jct.2008.10.002
66. D.G. Archer, R.W. Carter, Thermodynamic properties of the NaCl + H_2O system. 4. Heat capacities of H_2O and NaCl(aq) in cold-stable and supercooled states. J. Phys. Chem. B **104**, 8563–8584 (2000). https://doi.org/10.1021/jp0003914
67. C.A. Angell, M. Oguni, W.J. Sichina, Heat capacity of water at extremes of supercooling and superheating. J. Phys. Chem. **86**, 998–1002 (1982). https://doi.org/10.1021/j100395a032
68. M.J. Dávila, J.P.M. Trusler, Thermodynamic properties of mixtures of *N*-methyl-2-pyrrolidinone and methanol at temperatures between 298.15 K and 343.15 K and pressures up to 60 MPa. J. Chem. Thermodyn. **41**, 35–45 (2009). https://doi.org/10.1016/j.jct.2008.08.003
69. A. El Hawary. Schallgeschwindigkeitsmessungen in flüssigen Alkanen, Wasser und Krypton über weite Temperaturbereiche und unter hohen Drücken sowie abgeleitete Zustandsgrößen, Dr.-Ing. dissertation, Helmut-Schmidt-Universität/Universität der Bundeswehr Hamburg, Hamburg, Germany (2021). https://doi.org/10.24405/14016
70. W. Wagner, M. Thol, The behavior of IAPWS-95 from 250 to 300 K and pressures up to 400 MPa: evaluation based on recently derived property data. J. Phys. Chem. Ref. Data **44**, 043102 (2015). https://doi.org/10.1063/1.4931475
71. G. Tammann, W. Jellinghaus, Die Volumenisobaren des Wassers bis zur Schmelzkurve. Z. Anorg. Allg. Chem. **174**, 225–230 (1928). https://doi.org/10.1002/zaac.19281740123
72. P.W. Bridgman, The pressure-volume-temperature relations of the liquid, and the phase diagram of heavy water. J. Chem. Phys. **3**, 597–605 (1935). https://doi.org/10.1063/1.1749561
73. T. Grindley, J.E. Lind, *PVT* properties of water and mercury. J. Chem. Phys. **54**, 3983–3989 (1971). https://doi.org/10.1063/1.1675455
74. G.S. Kell, E. Whalley, Reanalysis of the density of liquid water in the range 0–150 °C and 0–1 kbar. J. Chem. Phys. **62**, 3496–3503 (1975). https://doi.org/10.1063/1.430986
75. G.S. Kell, G.E. McLaurin, E. Whalley, The PVT properties of water. IV. Liquid water in the range 150-350 °C, from saturation to 1 kbar. Proc. R. Soc. Lond. A **360**, 389–402 (1978). https://doi.org/10.1098/rspa.1978.0075
76. R. Hilbert, K. Tödheide, E.U. Franck, *PVT* data for water in the ranges 20 to 600°C and 100 to 4000 bar. Ber. Bunsenges. Phys. Chem. **85**, 636–643 (1981). https://doi.org/10.1002/bbpc.19810850906
77. J. Troncoso, The isobaric heat capacity of liquid water at low temperatures and high pressures. J. Chem. Phys. **147**, 084501 (2017). https://doi.org/10.1063/1.4990381
78. Y. Zheng, H. Gao, Q. Chen, X. Meng, J. Wu, Isobaric heat capacity measurements of liquid HFE-7200 and HFE-7500 from 245 to 353 K at pressures up to 15 MPa. Fluid Phase Equilibr. **372**, 56–62 (2014). https://doi.org/10.1016/j.fluid.2014.03.017
79. X. Zhao, Z. Liu, Z. Chen, Heat capacity for HFC152a/HFC32 mixture in liquid phase. J. Chem. Ind. Eng. (China) **49**, 740–744 (1998)
80. G. Ernst, R. Philippi, Flow-calorimetric results for the specific heat capacity c_p of water at pressures between 20 and 50 MPa and temperatures between 298.15 and 673.15 K. J. Chem. Thermodyn. **22**, 211–218 (1990). https://doi.org/10.1016/0021-9614(90)90085-5
81. Y.M. Naziev, M.M. Bashirov, Y.A. Badalov, Experimental study of isobaric specific heat of higher alcohols at high pressures. J. Eng. Phys. **51**, 1459–1464 (1986). https://doi.org/10.1007/BF00870363
82. A.M. Sirota, A.Y. Grishkov, A.G. Tomishko, Experimental study of the heat capacity of water near the melting curve. Teploenergetika **17**, 60–64 (1970)
83. T. Kuroki, N. Kagawa, H. Endo, S. Tsuruno, J.W. Magee, Specific heat capacity at constant volume for water, methanol, and their mixtures at temperatures from 300 K to 400 K and pressures to 20 MPa. J. Chem. Eng. Data **46**, 1101–1106 (2001). https://doi.org/10.1021/je0002437
84. J.W. Magee, R.J. Deal, J.C. Blanco, High-temperature adiabatic calorimeter for constant-volume heat capacity measurements of compressed gases and liquids. J. Res. Natl. Inst. Stand. Technol. **103**, 63–75 (1998). https://doi.org/10.6028/jres.103.003

85. I.M. Abdulagatov, V.I. Dvoryanchikov, A.N. Kamalov, Measurements of the heat capacities at constant volume of H_2O and (H_2O+KNO_3). J. Chem. Thermodyn. **29**, 1387–1407 (1997). https://doi.org/10.1006/jcht.1997.0248
86. E.W. Lemmon, I.H. Bell, M.L. Huber, M.O. McLinden, NIST Reference Fluid Thermodynamic and Transport Properties Database (REFPROP) Version 10.0, NIST Standard Reference Database 23, Standard Reference Data Program, National Institute of Standards and Technology, Gaithersburg, MD (2018)